0.70 (d, J = 6.0, Ir-CH_3); ^{2}H NMR (C_6H_6) δ -17.41 (d, J = 5.5, Ir-D).

Cp*(PMe_3)Ir(CD_3)D (6-d_4). This was prepared as above, except the deuterated chloro methyl complex, **5**-d_3, was treated with $NaBD_4$/LiCl: IR (C_6D_6) 1500 (br) cm^{-1}, ν_{Ir-D}; 2176, 2094, 2058 (m) cm^{-1}; ^{1}H NMR (C_6D_6) δ 1.87 (d, J = 1.5, $C_5(CH_3)_5$), 1.22 (d, J = 10.0, $P(CH_3)_3$); ^{2}H NMR (C_6H_6) δ 0.59 (d, J = 0.8, Ir-CD_3), -17.11 (d, J = 5.5, Ir-D). The material contained 4% Cp*(PMe_3)Ir(CD_3)H by NMR integration at long pulse delay.

Thermolysis of Cp*(PMe_3)Ir(CH_3)D (6-d_1). In the drybox, 8 and 10 mg of **6**-d_1 were loaded into each of two NMR tubes fused to ground glass joints. The tubes were protected from ambient light, attached to vacuum stopcocks and removed to a vacuum line. Degassed benzene-d_6 (0.7 mL) was added by vacuum transfer to both tubes, and to one was added trimethylphosphine (0.3 equiv by NMR integration). The tubes were sealed under vacuum and stored in the dark. No scrambling was observed after 24 h at room temperature in the dark. After the samples were heated at 125 °C for 18.5 h, ^{1}H NMR integration of both samples at long pulse delay indicated between 48 and 50% protium incorporation in the hydride position. After several days at 125 °C, the protium incorporation in the hydride position reached approximately 80%.

Thermolysis of Cp*(PMe_3)Ir(CH_3)H (6) with Cp*(PMe_3)Ir(CD_3)D (6-d_4). A degassed benzene-d_6 solution (1.0 mL) of methyl complexes **6** and **6**-d_4 (16 mg, 0.04 M each) and trimethylphosphine (0.5 eq) was heated to 160 °C in a sealed NMR tube. After 9 h, ^{1}H NMR analysis indicated a 65% conversion of starting materials to Cp*(PMe_3)Ir(C_6D_5)D (**2**-d_6) and Cp*Ir(PMe_3)D_2 in a ratio of approximately 3.5:1. The solution was frozen at -196 °C, the NMR tube cracked open in a sealed apparatus,[58] and the head gases sampled directly by MS. Analysis revealed the presence of all possible labeled methanes CH_nD_{4-n} (n = 0-4) in significant amounts.

(58) The apparatus used will be described: Wenzel, T. T.; Bergman, R. G. *J. Am. Chem. Soc.*, in press.

Acknowledgment. This work was carried out under the auspices of a collaborative Lawrence Berkeley Laboratory/Industrial research project supported Jointly by the Chevron Research Co., Richmond, CA, and the Director, Office of Energy Research, Office of Basic Energy Sciences, Chemical Sciences Division of the U.S. Department of Energy under Contract No. DE-AC03-76SF00098. J.M.S. acknowledges an NIH National Research Service Award (Grant No. F32-GM09289). Initial experiments to determine the equilibrium constant in the pentane-cyclohexane system were conducted by Dr. Caroline A. Kovac in these laboratories. The crystal structure analysis was performed by Dr. F. J. Hollander, staff crystallographer at the UC Berkeley X-ray crystallographic facility (CHEXRAY). Partial funding for the equipment in the facility was provided by the National Science Foundation through Grant No. CHE79-07027. The Bruker AM-500 NMR spectrometer was purchased with funds from NSF (No. CHE-8208994) and NIH (No. RR-02428) equipment grants. We are grateful to Mr. Rudi Nunlist for assistance in obtaining ^{1}H NMR spectra in hydrocarbon mixtures and to the Johnson-Matthey Co. for a loan of iridium trichloride. Tom Lawhead provided assistance in the design and fabrication of NMR sample tubes. The following individuals are thanked for the disclosure of results prior to publication: Profs. J. L. Beauchamp, R. H. Crabtree, J. Halpern, W. D. Jones, and J. R. Norton.

Supplementary Material Available: Crystal packing diagram for **1**, molecular geometry and labeling scheme for molecule **2**, hydrogen positional parameters and their estimated standard deviations, and listings of F_o and F_c (52 pages). Ordering information is given on any current masthead page.

Synthetic, Structural, and Theoretical Studies of η^2-Acyl Complexes of Molybdenum

M. David Curtis,* Kom-Bei Shiu, and William M. Butler

Contribution from the Department of Chemistry, The University of Michigan, Ann Arbor, Michigan 48109. *Received June 24, 1985*

Abstract: Hydridotris(pyrazolyl)borate (Tp) complexes of the type $TpMo(CO)_2(\eta^2\text{-COR})$ (R = Me (**1**), Ph (**2**)) are formed from the reaction of $TpMo(CO)_3^-$ with MeI, Me_3O^+, MeCOBr, or PhCOBr. The use of ^{13}C-labeled PhC*OBr in the reaction established that a carbonyl initially on the metal is lost in the decarbonylation and that the η^2-acyl is not in equilibrium with a low concentration of the isomeric σ-alkyltricarbonyl complex. The derivatives $Tp(CO)LMo(\eta^2\text{-COMe})$ (L = $P(OMe)_3$ (**3**) and PEt_3 (**4**)) are made from **1** and the appropriate phosphine. The structures of **1**-**4** were determined by X-ray crystallography: (**1**) a, b, and c = 8.995 (3), 12.803 (4), and 14.999 (6) Å; β = 103.98 (3)°; V = 1677 (1) Å^3; Z = 4; space group $P2_1/n$ (no. 14); (**2**) a, b, and c = 9.405 (2), 12.505 (3), and 9.025 (2) Å; α, β, and γ = 114.59 (2), 92.85 (2), and 95.45 (2)°; V = 956.0 (4) Å^3; Z = 2; space group = $P\bar{1}$ (no. 2); (**3**) a, b, and c = 8.953 (2), 15.684 (6), and 8.032 (4) Å; α, β, and γ = 99.47 (4), 102.79 (3), and 97.78 (3)°; V = 1067.5 (7) Å^3; Z = 2; space group = $P\bar{1}$. Values of R_1 and R_2 for **1**-**4** are 0.045, 0.059 (**1**); 0.038, 0.063 (**2**); 0.038, 0.056 (**3**); and 0.044, 0.061 (**4**). The bonding of an L_5M (d^4) fragment to the η^2-acyl group, the rotational conformations of the latter, and the relative stabilities of $Cp(CO)_2Mo(\eta^2\text{-HCO})$, $Cp(CO)_3Mo\text{-H}$, $(N\text{-donor})_3(CO)_2Mo(\eta^2\text{-HCO})$, and $(N\text{-donor})_3(CO)_3Mo\text{-H}$ are comprehensively treated within the framework of the Extended Hückel MO formalism. It is shown that there is substantial double-bond character in the Mo=C(acyl) bond but a very weak Mo—O bond and that the compounds should be regarded as stabilized 16-electron complexes. There is an inherent tendency toward a bending distortion in the L_5M fragment, and the η^2-acyl group tends to be aligned with the axis of distortion and/or with the M—CO bond(s).

The preparation of η^2-acyl complexes and their chemical properties have been the subject of much recent research.[1-11] This interest is derived in part from the possible role of η^2-acyl and η^2-formyl structures in metal-catalyzed hydrogenation of carbon

(1) (a) Fachinetti, G.; Fochi, G.; Floriani, C. *J. Chem. Soc. Dalton Trans.* **1977**, 1946. (b) Fachinetti, G.; Floriani, C.; Stockli-Evans, H. *Ibid.* **1977**, 2297. (c) Fachinetti, G.; Floriani, C.; Marchetti, F.; Medino, S. *J. Chem. Soc., Chem. Commun.* **1976**, 522.

(2) (a) Erker, G.; Rosenfeldt, F. *Angew. Chem., Int. Ed. Engl.* **1978**, *17*, 605. (b) *J. Organomet. Chem.* **1980**, *188*, C1.

(3) Strauss, O. A.; Grubbs, R. H. *J. Am. Chem. Soc.* **1982**, *104*, 5499.

(4) Marsella, J. A.; Caulton, K. G. *J. Am. Chem. Soc.* **1980**, *102*, 1747.

0002-7863/86/1508-1550$01.50/0

monoxide.[12-15] Most of the η^2-formyl and η^2-acyl complexes synthesized to date make use of the oxophilic character of early transition elements, e.g., group 4, or of lanthanides and actinides in the +4 oxidation states to stabilize the η^2-bonding mode of the COR group. Two other means of promoting alkyl group migration to coordinated CO have been found. These are oxidatively promoted migration, wherein the M(CO)R complex is oxidized by one electron,[16,17] and Lewis acid assisted migration in which the acid complexes to the carbonyl oxygen.[18-20]

Outside of the actinides and the group 4 metals, relatively few mononuclear η^2-acyl complexes have been reported. At the inception of this work, only one η^2-acyl complex of Mo, $[(\mu\text{-Cl})(PMe_3)(CO)_2(\eta^2\text{-}COCH_2SiMe_3)Mo]_2$, was known,[21] although several others, viz., $Mo(PMe_3)_3Cl(CO)(\eta^2\text{-COR})$,[22a] its derivatives and tungsten analogues,[22b] and $Tp^*Mo(CO)_2(\eta^2\text{-COR})$[23] ($Tp^*$ = hydridotris(3,5-dimethylpyrazolyl)borato), were reported during the course of this work. Weiss et al.[24] have prepared a series of η^2-acyls of vanadium, $V(CO)_3(\eta^2\text{-COR})(LL)$ (LL = chelating bis(phosphine) or bis(arsine)), and Roper[25] and co-workers have reported a ruthenium η^2-acyl, $(Ru(\eta^2\text{-COMe})I(CO)(PMe_3)_2)$, which is in equilibrium with its (carbonyl)(σ-alkyl) isomer.

In this paper, we report that the electronic and steric demands of the hydridotris(pyrazolyl)borate (Tp) ligand also promotes facile migratory CO insertion and decarbonylations to give η^2-acyl complexes. The structures of these complexes and two phosphine adducts are presented, and the bonding of the η^2-acyl group to d^4 L_5M fragments is discussed with the aid of EHMO calculations.

Experimental Section

General. All manipulations were performed under an atmosphere of prepurified nitrogen in an inert atmosphere box with recirculating purification train or with Schlenk techniques. Solvents were dried, degassed, and distilled prior to use. $[Et_4N][TpMo(CO)_3]$ was prepared as reported previously.[26] Benzoyl bromide labeled with ^{13}C at the carbonyl carbon, PhC*OBr, was prepared from PhC*O_2H, 90% enriched with ^{13}C and obtained from Stohler Isotopes, Inc., by a published procedure.[27]

Elemental analyses were performed by Galbraith or Schwartzkopf Laboratories. NMR spectra were recorded on a Bruker WM360 spectrophotometer (360 MHz for ^1H and 90.56 MHz for ^{13}C). Chemical shifts are in ppm vs. TMS. IR spectra were obtained on a Perkin-Elmer Model 1330 instrument, and peak positions were calibrated with polystyrene film. All the *neutral* Tp metal complexes displayed a B-H stretching band near 2500 cm^{-1}. Mass spectra were obtained with the direct insert probe of a Finnegan 4021 quadrupole mass spectrometer operated in the chemical ionization (CH_4^+) mode.

$TpMo(CO)_2(\eta^2\text{-CoMe})$ (1). Method 1. MeI (7.0 mL, 110 mmol) was added to 100 mL of acetonitrile in which 13.7 g (26.3 mmol) of $[Et_4N][TpMo(CO)_3]$ had been dissolved. This mixture was refluxed for 0.5 h, and the solvent was removed under vacuum. The brown residue was extracted with 200 mL of ether in a Soxhlet extractor until the extract was pale red (about 10 h). The volume of the extract was reduced to 10 mL to give 8.8 g (83%) of brick-red crystals, mp 184-185 °C dec.

The above procedure may be modified by substituting the Soxhlet extraction as follows. The brown residue was dissolved in 80 mL of CH_2Cl_2 and the solution filtered. MeOH (30 mL) was added to the filtrate, and most of the CH_2Cl_2 was pumped off under reduced pressure. The resulting suspension was cooled to −40 °C and filtered cold to give **1** (60%). Anal. Calcd for $C_{13}H_{13}BMoN_6O_3$: C, 38.26; H, 3.21. Found: C, 38.15; H, 3.60. MS M, (M − CO), (M − Me), (M − Me − CO), (M − 2CO), (M − Me − 2CO), (M − 3CO), and (M − Me − 3CO) (M = parent ion); IR (KBr) 1983 (s), 1856 (s), 1510 (w); IR (CH_2Cl_2 solution) 1980 (s), 1850 (s), 1513 (w); ^1H NMR(CD_2Cl_2) 7.73 (d, A), 7.69 (d, B) (H_3); 7.58 (d, A), 7.41 (d, B) (H_5); 6.20 (t, A), 6.19 (t, B, $^3J_{H_3H_4}$ = 2.3 Hz, $^3J_{H_5H_4}$ = 1.8 Hz, A:B = 1:2 (H_4); 3.23 (s, Me); gated ^{13}C NMR (CD_2Cl_2) 147 (d, A), 143 (d, B) (C_3, $^1J_{CH}$ = 185 Hz); 137 (d, A), 136 (d, B) (C_5, $^1J_{CH}$ = 188 Hz), 107 (d, A), 106 (d, B) (C_4, $^1J_{CH}$ = 178 Hz) (A:B = 1:2), 236 (s, CO), 268 (q, COMe, $^2J_{CH}$ = 6 Hz), 28.0 (q, (Me, $^1J_{CH}$ = 131 Hz). Essentially the same spectrum was obtained in CD_2Cl_2/diglyme from −93 to +72 °C.

Method 2. Equimolar amounts of $[Et_4N][TpMo(CO)_3]$ and $[Me_3O]BF_4$ (1.9 mmol) were placed in a flask held at −78 °C. Prechilled CH_2Cl_2 (−78 °C) was added and the solution stirred at −78 °C for 2 h. No reaction (color change) was apparent. The mixture was then allowed to warm to room temperature at which point the IR spectrum showed complete conversion to **1**.

Reactions of $TpMo(CO)_3^-$ with RCOX. RCOX = MeCOBr. Acetyl bromide (0.45 mL) was added to a solution of $[Et_4N][TpMo(CO)_3]$ (1.94 g, 3.71 mmol) in 20 mL of CH_3CN. The mixture was stirred at room temperature for 1.5 h after which time some orange solid had formed. This suspension was filtered to give 0.91 g (39%) of orange solid **5**, identified as $[Et_4N][MoBr_4(MeCN)_2]$ (see below). The solvent was removed from the filtrate under vacuum, and the residue was extracted with 100 mL of ether until the extract was pale red. The ether solution was then concentrated to yield 0.33 g (22%) of **1**.

The orange solid, **5**, melted at 203 °C dec. It is not soluble in common organic solvents: IR (KBr) (ν_{CN}) 2285 (s), 2330 (s). Anal. Calcd for $C_{12}H_{26}Br_4MoN_3$: C, 22.95; H, 4.17; Mo, 15.28; Br, 50.90; N, 6.69. Found: C, 22.88; H, 4.13; Mo, 15.22; Br, 51.01; N, 6.86.

RCOX = PhCOBr. Three milliliters of PhCOBr was added to a solution of 2.61 g (4.99 mmol) of $[Et_4N][TpMo(CO)_3]$ in 60 mL of acetonitrile. Gas evolution was noted, and after 20 min, an IR spectrum of the dark solution showed complete consumption of the $TpMo(CO)_3^-$ anion. The solvent was removed under reduced pressure and the residue was treated with 50 mL of ether. The ether solution was filtered and the ether removed from the filtrate under reduced pressure to give the dark-blue product, mp 224 °C dec: yield 0.53 g (23%). The finely divided solid is pyrophoric when dry. Anal. Calcd for $C_{18}H_{15}BMoN_6O_3$: C, 45.99; H, 3.22. Found: C, 45.02; H, 3.24. MS M, (M − CO), (M − CO − Ph), (M − 2CO), and (M − 3CO) (M = parent ion); IR (KBr) 1993 (s), 1838 (s), 1490 (w); IR (CH_2Cl_2) 1965 (s), 1852 (s), 1490 (w). ^1H NMR ($CDCl_3$) 7.76 (d, A), 7.71 (d, B) (H_3); 7.69 (d, A), 7.47 (d, B) (H_5); 6.17 (t, A), 6.25 (t, B, $^3J_{H_3H_4}$ = 1.7, $^3J_{H_4H_5}$ = 1.4 Hz), A:B = 1:2 (H_4); 7.69 (m, Ph); ^{13}C NMR ($CDCl_3$) 145 (A), 143 (B) (C_3); 136 (A), 135 (B) (C_5); 106 (A), 105 (B) (C_4); 239 (CO); 254 (COPh); 134, 131, 129, 128 (Ph).

RCOX = PhC*OBr. The above procedure was repeated by using 1.1 g of $[Et_4N][TpMo(CO)_3]$ and 0.25 mL of PhC*OBr (90% ^{13}C-enriched) in 10 mL of acetonitrile. The product displayed ν_{CO} bands at 1963 (s), 1850 (s), and 1455 (w) in CH_2Cl_2. The isotope shift (35 cm^{-1}) of the acyl C-O stretch is nearly identical with that calculated (38 cm^{-1}) for a harmonic, two-atom vibrator.

Attempted Formation of $TpMo(CO)_2(\eta^2\text{-HCO})$. $TpMo(CO)_2H$ (0.68 g) was dissolved in either DMF or diglyme and the solution heated to reflux. After several hours, IR spectra of the solutions showed the dis-

(5) Marsella, J. A.; Huffman, J. C.; Caulton, K. G.; Longato, B.; Norton, J. R. *J. Am. Chem. Soc.* **1982**, *104*, 6360.
(6) Labinger, J. A.; Miller, J. S. *J. Am. Chem. Soc.* **1982**, *104*, 6856.
(7) Belmonte, P. A.; Cloke, F. G. N.; Shrock, R. R. *J. Am. Chem. Soc.* **1983**, *105*, 2643.
(8) Pearson, R. G.; Walker, H. W.; Mauermann, H.; Ford, P. C. *Inorg. Chem.* **1981**, *20*, 2743.
(9) Kropp, K.; Skilbe, V.; Erker, G.; Krüger, C. *J. Am. Chem. Soc.* **1983**, *105*, 3353.
(10) Moore, E. J.; Straus, D. A.; Armantrout, J.; Santarsiero, B. D.; Grubbs, R. H.; Bercaw, J. E. *J. Am. Chem.* Soc. **1983**, *105*, 2068.
(11) (a) Moloy, K. G.; Marks, T. J. *J. Am. Chem. Soc.* **1984**, *106*, 7051. (b) Sonnenberger, D. C.; Mintz, E. A.; Marks, T. J. *Ibid.* **1984**, *106*, 3484.
(12) Masters, C. *Adv. Organomet. Chem.* **1979**, *17*, 61.
(13) Muetterties, E. L.; Stein, J. *Chem. Rev.* **1979**, *79*, 479.
(14) Rofer-De Poorter, C. K. *Chem. Rev.* **1981**, *81*, 447.
(15) Herrmann, W. A. *Angew. Chem., Int. Ed. Engl.* **1982**, *21*, 117.
(16) Cameron, A.; Smith, V. H.; Baird, M. C. *Organometallics* **1983**, *2*, 465.
(17) Magnuson, R. H.; Meirowitz, R.; Zulu, S.; Giering, W. P. *J. Am. Chem. Soc.* **1982**, *104*, 5790.
(18) Richmond, T. G.; Basolo, F.; Shriver, D. F. *Inorg. Chem.* **1982**, *21*, 1272.
(19) Labinger, J. A.; Bonfiglio, J. N.; Grimmeth, D. L.; Masuo, S. T.; Shearin, E.; Miller, J. S. *Organometallics* **1983**, *2*, 733.
(20) La Croce, S. J.; Cutler, A. R. *J. Am. Chem. Soc.* **1982**, *104*, 2312.
(21) Guzman, E. C.; Wilkinson, G.; Rogers, R. D.; Hunter, W. E.; Zaworotko, M. J.; Atwood, J. L. *J. Chem. Soc., Dalton Trans.* **1980**, 229.
(22) (a) Carmona, E.; Sanchez, L.; Marin, J. M.; Poveda, M. L.; Atwood, J. L.; Priester, R. D.; Rogers, R. D. *J. Am. Chem. Soc.* **1984**, *104*, 3214. (b) Carmona, E.; Marin, J. M.; Poveda, M. L.; Sanchez, L.; Rogers, R. D.; Atwood, J. L. *J. Chem. Soc., Dalton Trans.* **1983**, 1003.
(23) Desmond, T.; Lalor, F. J.; Ferguson, G.; Ruhl, B.; Parvey, M. *J. Chem. Soc., Chem. Commun.* **1983**, 55.
(24) (a) Franke, U.; Weiss, E. *J. Organomet. Chem.* **1979**, *165*, 329. (b) Schiemann, J.; Weiss, E. *Ibid.* **1983**, *255*, 179.
(25) Roper, W. R.; Taylor, G. E.; Waters, J. M.; Wright, L. J. *J. Organomet. Chem.* **1979**, *182*, C46.
(26) Curtis, M. D.; Shiu, K.-B. *Inorg. Chem.* **1985**, *24*, 1213.
(27) Bestmann, H. J.; Mott, L. *Ann. Chem.* **1966**, *693*, 132.

appearance of starting material and new bands at 2438 (s), 1880 (s) and 1735(s) cm^{-1}. The solvents were removed under reduced pressure to give a tacky oil with the same IR bands as observed in solution. The tacky material could not be crystallized and was not characterized further. It was also found that simple dissolution of the hydride in DMF or diglyme gave IR bands characteristic of the anion $TpMo(CO)_3^-$.

$TpMo(CO)(\eta^2$-COMe)$(P(OMe)_3)$. To a toluene solution (120 mL) containing 0.98 g (2.4 mmol) of **1** was added 5 mL of $P(OMe)_3$. The solution was heated to reflux for 4 h after which time the volume was reduced to 20 mL under reduced pressure. The concentrated solution was cooled to −20 °C overnight and filtered to give 0.66 g (55%) of orange-red product, mp 163 °C dec. Anal. Calcd for $C_{15}H_{22}BMoN_6O_5P$: C, 35.74; H, 4.40. Found: C, 35.54; H, 4.43. MS M, (M − OMe), (M − CO − Me), (M − $P(OMe)_3$), (M − 2CO − Me), (M − CO − OMe), (M − 2CO − OMe), (M − Me − $P(OMe)_3$), (M − CO − $P(OMe)_3$) (M = parent ion); IR (KBr) 1803 (s), 1508 (w); IR (CH_2Cl_2) 1800 (s), 1508 (w); ^1H NMR (CD_2Cl_2) 7.89 (d, D), 7.80 (d, E), 7.79 (d, F) (H_3); 7.66 (d, D), 7.59 (d, E), 7.00 (d, F) (H_5); 6.34 (t, D), 6.24 (t, E), 6.04 (t, F, $^3J_{H_3H_4}$ = 2.2, $^3J_{H_4H_5}$ = 1.7 Hz), D:E:F = 1:1:1 (H_4); 3.26 (d, O*Me*, $^3J_{PH}$ = 11 Hz); 3.00 (d, CO*Me*, $^4J_{PH}$ = 1 Hz); ^{13}C NMR (CH_2Cl_2/toluene-d_8, 3:1, −75 °C) 267.6 (d, η^2-*C*OMe, $^2J_{PC}$ = 48 Hz); 236.4 (d, *C*O, $^2J_{PC}$ = 14 Hz); 147.4 (A), 143.6 (A), 142.4 (A) (C_3); 135.1 (B), 136.6 (A) (C_5); 105.8 (B), 105.0 (A) (C_4) (A:B = 1:2); 50.6 (PO*Me*); 28.2 (η^2-CO*Me*).

$TpMo(CO)(\eta^2$-COMe)PEt_3. Toluene (100 mL), **1** (0.99 g, 2.43 mmol), and PEt_3 (0.80 mL, 5.48 mmol) were added to a 250-mL flask, and the solution was refluxed for 14 h after which time the IR spectrum showed complete consumption of **1**. The solvent and excess phosphine were removed under reduced pressure to give an orange residue. The residue was taken up in 10 mL of CH_2Cl_2. Acetonitrile (20 mL) was added to the solution, the volume of which was then reduced to 3 mL under vacuum. Orange crystals (0.90 g, 74%), mp 175–177 °C dec, were obtained. Anal. Calcd for $C_{18}H_{28}BMoN_6O_2P$: C, 43.40; H, 5.67. Found: C, 43.52; H, 5.70. MS M^+, (M − Me), (M − CO − Me), (M − 2CO − Me), (M − PEt_3 − CO), (M − PEt_3 − Me), (M − PEt_3 − CO − Me), (M − CO), (M − 2CO), (M − PEt_3 − 2CO), (M − PEt_3 − 2CO − Me) (M = parent ion); IR (KBr) 1775 (s), 1498 (w); IR (CH_2Cl_2) 1765 (s), 1510 (w); ^1H NMR (CD_3CN) 8.32 (d, D), 7.84 (d, E), 7.10 (d, F) (H_5); 7.74 (d, D), 7.68 (d, E), 7.67 (d, F) (H_3); 6.28 (t, D), 6.23 (t, E), 6.11 (t, F, $^3J_{H_3H_4}$ = 2.1, $^3J_{H_4H_5}$ = 1.7 Hz), D:E:F = 1:1:1 (H_4); 2.70 (s, CO*Me*); 1.98 (s, B*H*); 1.84 (dq, CH_2, $^2J_{PH}$ = 20 Hz); 0.66 (dt, CH_3, $^3J_{PH}$ = 14, $^3J_{HH}$ = 7.5 Hz); ^{13}C NMR (CH_2Cl_2/toluene-d_8, 3:1) 253.6 (*C*OMe); 201.3 (*C*O); 145.7 (A), 144.6 (A), 139.2 (A), 135.7 (A), 134.9 (B), 105.3 (A), 105.0 (A), 104.8 (A), ring carbons, A:B = 1:2; 16.3 (d, P*C*H_2, $^1J_{PC}$ = 20 Hz); 6.6 (PC*C*H_3). The peak due to the acetyl methyl was not observed. It most likely was buried beneath the peak due to the toluene-d_8–methyl resonance (~20–21 ppm).

The filtrate from the orange crystals obtained as above was chromatographed over a 2 × 32 cm column packed with alumina. Toluene eluted a green band from which 0.01 g (12%) of green solid identified as $Tp_2Mo_2(CO)_4$ was obtained.[28,29]

Reaction of 1 with I_2. Iodine (0.32 g, 1.25 mmol) was added to 0.50 g (1.23 mmol) of **1** dissolved in 30 mL of CH_2Cl_2. After 6 h, the IR spectrum of the solution showed the complete conversion of **1** to $TpMo(CO)_3I$. The identity of the product was confirmed by its isolation and comparison to authentic $TpMo(CO)_3I$ prepared by an alternate route.[26]

X-ray Structure Determinations. Crystals of $TpMo(CO)_2(\eta^2$-COMe) (**1**), $TpMo(CO)_2(\eta^2$-COPh) (**2**), $TpMo(CO)(\eta^2$-COMe)$P(OMe)_3$ (**3**), and $TpMo(CO)(\eta^2$-COMe)PEt_3 (**4**) were grown from toluene at room temperature, CH_2Cl_2/hexane at room temperature, CH_2Cl_2/hexane at −20 °C, and toluene/hexane at room temperature, respectively. Crystals of **1** and **2** were mounted on a glass fiber in air, but those of **3** and **4** were sealed in 0.2-mm glass capillaries. Diffraction data were collected at room temperature (21 ± 1 °C).

Cell dimensions were obtained from the settings of 15 refined reflections distributed in reciprocal space. Systematic absences, if present, were determined from small, low-angle data sets. All the structures were solved by locating the Mo atom in a 3D Patterson map and by locating the remaining non-hydrogen atoms in subsequent difference maps. The structures were refined to convergence with isotropic temperature factors for all atoms and then to convergence with anisotropic temperature factors. The final difference maps showed maxima (0.5–1.0 e/Å^3) in positions expected for hydrogen atoms, but these were not included in the structure. No other significant peaks were observed. The maximum shift/error for any variable on the last refinement cycle was less than 1.0.

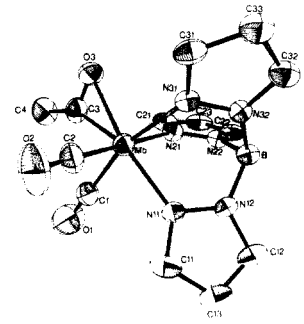

Figure 1. ORTEP plot of $TpMo(CO)_2(\eta^2$-COMe) (**1**).

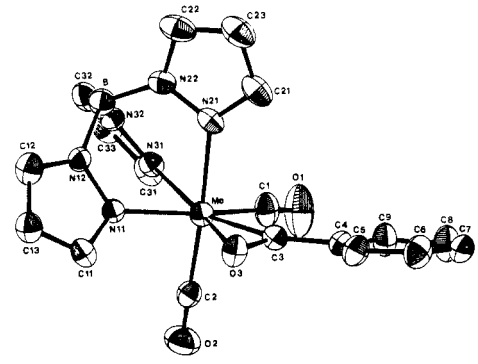

Figure 2. ORTEP plot of $TpMo(CO)_2(\eta^2$-COPh) (**2**).

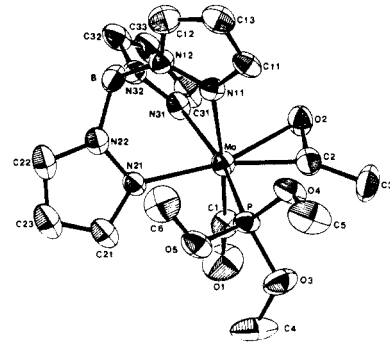

Figure 3. ORTEP plot of $TpMo(CO)(P(OMe)_3)(\eta^2$-COMe) (**3**).

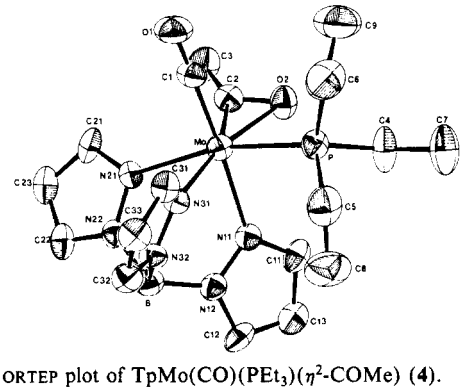

Figure 4. ORTEP plot of $TpMo(CO)(PEt_3)(\eta^2$-COMe) (**4**).

All programs, sources for scattering factors, etc., have been described elsewhere.[26]

Crystals and refinement statistics are collected in Table I, fractional atomic coordinates are listed in Table II, and selected bond lengths and bond angles are in Tables III and IV, respectively. Complete listings of bond lengths, angles, and tables of F_o vs. F_c are included in the supplementary material. ORTEP plots of the molecular structures with the numbering schemes are shown in Figures 1–4 (thermal ellipsoids are drawn at the 50% probability level).

Results and Discussion

Syntheses. It was reported originally that the reaction of $TpMo(CO)_3^-$ with MeI gave the σ-methyl complex, TpMo-

(28) Shiu, K.-B.; Curtis, M. D.; Huffman, J. C. *Organometallics* **1983**, *2*, 936.

(29) Curtis, M. D.; Shiu, K.-B.; Butler, W. M.; Huffman, J. C. *J. Am. Chem. Soc.*, in press.

Table I Crystal Data for $TpMo(CO)(L)(\eta^2\text{-COR})$: R = Me and Ph; L = CO, $P(OMe)_3$, and PEt_3

	1	2	3	4
$TpMo(Co)(L)(^2\text{-COR})$	R = Me, L = CO	R = Ph, L = CO	R = Me, L = P $(OMe)_3$	R = Me, L = PEt_3
fw, g/mol	408.04	470.11	504.10	498.18
color	brick-red	dark blue	orange–red	orange
ρ_{calcd}, g/mL	1.617	1.633	1.568	1.466
ρ_{found}, g/mL		1.63 ($ZnBr_2H_2O$)	1.56 ($ZnBr_2/H_2O$)	
radiation	Mo Kα	Mo Kα	Mo Kα	Mo Kα
cell dimensions				
a, Å	8.995 (3)	9.405 (2)	8.953 (2)	8.040 (3)
b, Å	12.803 (4)	12.505 (3)	15.684 (6)	8.850 (4)
c, Å	14.999 (6)	9.025 (2)	8.032 (4)	16.517 (6)
α, deg	90.00 (3)	114.59 (2)	99.47 (4)	96.81 (3)
β, deg	103.98 (3)	92.85 (2)	102.79 (3)	100.12 (3)
γ, deg	90.00 (3)	95.45 (2)	97.78 (3)	99.32 (3)
V, Å^3	1677 (1)	956.0 (4)	1067.5 (7)	1128.6 (9)
space group	$P2_1/n$ (no. 14)	$P\bar{1}$ (no. 2)	$P\bar{1}$ (no. 2)	$P\bar{1}$ (no. 2)
Z	4	2	2	2
$2\theta_{max}$, deg	50	45	45	45
crystal dimensions	0.28 × 0.05 × 0.20 mm	0.41 × 0.20 × 0.40 mm	0.18 × 0.18 × 0.33 mm	0.185 × 0.38 × 0.19 mm
std. reflections	(400)	(211)	(3$\bar{1}\bar{1}$)	(2$\bar{1}$1)
	(061)	(2$\bar{4}$2)	(2$\bar{5}$1)	(2$\bar{3}$1)
	(006)	(10$\bar{3}$)	(20$\bar{2}$)	(12$\bar{5}$)
μ, cm^{-1}	7.856	7.001	7.091	6.609
I_{max}, I_{min}	0.961, 0.803	0.869, 0.750	0.880, 0.791	0.879, 0.778
N, NO, NV	3533, 2045, 217	2683, 2360, 262	3005, 2241, 262	3163, 2175, 262
R_1, R_2	0.045, 0.059	0.038, 0.063	0.038, 0.056	0.044, 0.061
GOF	1.12	2.87	2.62	1.69

Scheme I[a]

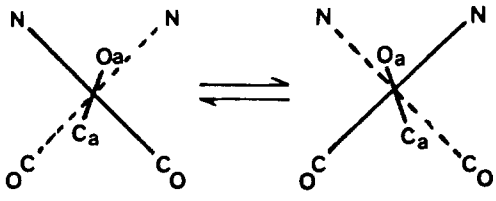

(1)

[a] N trans to the acyl group is not drawn for clarity. The bonds drawn with dashed lines are bent down below the plane of the paper.

$(CO)_3Me$.[30] We had occasion to repeat this synthesis and noticed that the brick-red product exhibits two ν_{CO} bands with nearly equal intensities at 1983 and 1856 cm^{-1}. This pattern is unlike those of seven-coordinate $TpMo(CO)_3X$ (X = H, Br, and I) complexes having C_s symmetry and displaying three ν_{CO} bands (2A′ + A″) in the IR.[26] Furthermore, we noted a weak, previously unreported band at 1510 cm^{-1} which is not present in the $TpMo(CO)_3X$ complexes.

An X-ray structure determination of this product revealed that it is in fact the η^2-acetyl complex, $TpMo(CO)_2(\eta^2\text{-COMe})$, **1** (Figure 1). The gated $^{13}C\{^1H\}$ NMR spectrum of **1** is consistent with its formulation as an η^2-acetyl complex in solution. The two terminal carbonyls show a single resonance at 236 ppm and the acyl carbon resonance is a quartet ($^2J_{CH}$ = 6 Hz) centered at 265 ppm. The acetyl methyl carbon appears as a quartet ($^1J_{CH}$ = 131 Hz) at 28 ppm. If the solid-state structure (see below) were maintained in solution, two resonances, one each for the nonequivalent carbonyls, would be expected. However, only one carbonyl resonance is observed down to −93 °C. The three pyrazolyl (pz) rings appear as two sets in a 1:2 ratio rather than the expected three. Hence, a low-energy fluxional process is indicated which time-averages the effective symmetry to C_s. The minimal motion which time-averages the molecule to C_s symmetry is a libration of the η^2-COMe group coupled with a bending motion as shown in Scheme I. The barrier calculated for this motion is quite low (see discussion of EHMO results below).

The reaction of $TpMo(CO)_3^-$ with MeI requires elevated temperature for rapid reaction and it was thought that the σ-methyl complex, $TpMo(CO)_3Me$ (**6**), may have formed and rearranged to the η^2-acetyl **1** in the hot acetonitrile. In order to effect reaction at a lower temperature, $TpMo(CO)_3^-$ was allowed to react with $Me_3O^+BF_4^-$ at −78 °C. There was no apparent reaction, but as the solution was allowed to warm to room temperature, the characteristic red color of **1** developed. The IR spectrum of the solution obtained at room temperature showed the presence of only **1**. Thus, if **6** is formed at all, it rapidly rearranges to **1** (eq 2).

$$TpMo(CO)_3^- + MeX \xrightarrow{-X^-} \underset{\mathbf{6}}{[TpMo(CO)_3\text{–}Me]} \rightarrow \underset{\mathbf{1}}{TpMo(CO)_2(\eta^2\text{-COMe})} \quad (2)$$

It is pertinent to note that Desmond et al.[23] have recently determined that the intensely colored products[31] resulting from the reaction of $Tp^*Mo(CO)_3^-$ and ArN_2^+ are the corresponding $Tp^*Mo(CO)(\eta^2\text{-COAr})$ η^2-acyl complexes. Furthermore, these workers have convincingly demonstrated that these reactions proceed by a redox mechanism which produces the $Tp^*Mo(CO)_3$· and Ar· radicals. We have found no evidence which suggests that the reaction of $TpMo(CO)_3^-$ with MeI or Me_3O^+ proceeds by a free-radical mechanism. In particular, no carbyne products have been found when the reactions are run in the presence of CH_2Cl_2 in contrast to the results of Desmond et al. who found that $Tp^*Mo(CO)_2(\equiv CCl)$ is formed from the reaction of $Tp^*Mo(CO)_3^-$ with ArN_2^+ or Ph_2I^+ in the presence of CH_2Cl_2.[32] Furthermore, we have never observed η^2-acyl complexes, $TpMo(CO)_3(COR)$, in which the R group was derived from a solvent-based radical.[23]

A difference in reactivity between $TpMo(CO)_3^-$ and $Tp^*Mo(CO)_3^-$ is also observed in their reactions with ArN_2^+. The former gives the substitution product,[33] $TpMo(CO)_2(N_2Ar)$, while the latter yields the η^2-acyl or carbyne complexes described above. The difference in reactivity between the Tp and Tp* complexes may be related to two factors. First, the electron-releasing methyl groups in the Tp* ligand may reduce the oxidation potential of the $Tp^*Mo(CO)_3^-$ anion relative to that of $TpMo(CO)_3^-$. Second, the increased steric bulk of the Tp* ligand may hinder simple substitution reactions of $Tp^*Mo(CO)_3^-$ to the point that free-radical processes may compete.

(30) Trofimenko, S. *J. Am. Chem. Soc.* **1969**, *91*, 588.

(31) Trofimenko, S. *Inorg. Chem.* **1971**, *10*, 504.

(32) Desmond, T.; Lalor, F. J.; Ferguson, G.; Parvez, M. *J. Chem. Soc., Chem. Commun.* **1983**, 457.

(33) (a) Trofimenko, S. *Inorg. Chem.* **1969**, *8*, 2675. (b) Condon, D.; Ferguson, G.; Lalor, F. J.; Parvez, M. *Ibid.* **1982**, *21*, 188.

Since $CpMo(CO)_3^-$ reacts readily with acyl halides, RCOX, we were interested in determining the course of the reaction of $TpMo(CO)_3^-$ wiith acyl halides. Would the σ-acyl, **7**, rearrange to **8** in a fashion similar to the alkyl migration depicted in eq 3 (cf. eq 2)?

$$TpMo(CO)_3^- + RCOX \longrightarrow \underset{\mathbf{7}}{Tp(CO)_3Mo(\sigma\text{-}COR)} \longrightarrow \underset{\mathbf{8}}{Tp(CO)_2Mo(\eta^2\text{-}COR)} \quad (3)$$

It was found that $TpMo(CO)_3^-$ did not react with MeCOCl in refluxing acetonitrile. The anion did react with MeCOBr, however, to give a 22% yield of **1** and a 39% yield of $[Et_4N][MoBr_4(NCMe)_2]$ (**5**). The two strong ν_{CN} bands at 2285 and 2330 cm^{-1} of the latter complex establish that the coordinated acetonitriles are cis (eq 4). The mechanism of the oxidation leading to **5** and the reduction product(s) is not known.

$$TpMo(CO)_3^- + MeCOBr \rightarrow \underset{\mathbf{1}}{TpMo(CO)_2(\eta^2\text{-}COMe)} + \underset{\mathbf{5}}{cis\text{-}MoBR_4(NCMe)_2^-} \quad (4)$$

The reaction of $TpMo(CO)_3^-$ with PhCOBr gave a 23% yield of the η^2-benzoyl complex, **2**. When this reaction was repeated with PhC*OBr, 90% enriched with ^{13}C at the acyl carbon, the product contained the label only in the η^2-benzoyl group. This experiment demonstrates two things. First, the carbonyl which is lost was originally on the metal, and second, the η^2-benzoyl complex is not in equilibrium with a low concentration of the σ-phenyl complex as shown in eq 5.

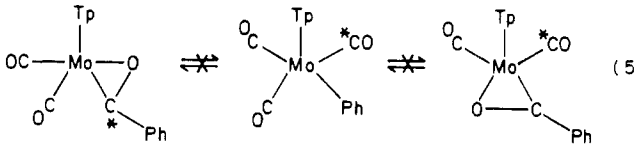

(5)

The η^2-benzoyl complex **2** is fluxional in solution. The ^1H and ^{13}C NMR spectra of **2** reveal the same time-averaged C_s symmetry as found for **1**. Both terminal carbonyls give a single resonance at 239 ppm and the acyl carbon resonates at 254 ppm.

The facile alkyl to CO migration shown in eq 2 and the decarbonylation reactions shown in eq 4 hve no precedent in the chemistry of $CpMo(CO)_3R$ or $CpMo(CO)_3(\sigma\text{-}COR)$. The σ-methyl complex is relatively stable and does not react with CO even at 316 atm ($T < 55$ °C).[34] In the presence of $AlBr_3$, $CpMo(CO)_3Me$ undergoes rapid methyl migration to give the cyclic acyl–$AlBr_3$ adduct, $Cp(CO)_2Mo[C(OAlBrBr_2)Me]$, which is hydrolyzed to the σ-acetyl complex, $CpMo(CO)_3(\sigma\text{-}COMe)$.[35] Upon heating, the latter decomposes to $CpMo(CO)_3Me$ and other unidentified products. $CpMo(CO)_3(\sigma\text{-}COPh)$[36] and $CpMo(CO)_3Et$[37] are reported to decompose to $(RC_5H_4)_2Mo_2(CO)_6$ (R = Ph and Et) or $Cp_2Mo_2(CO)_6$ depending on the conditions.

Thus, in the Cp series, the order of stability appears to be $CpMo(CO)_3R > CpMo(CO)_3(\sigma\text{-}COR) \gg CpMo(CO)_2(\eta^2\text{-}COR)$ (the latter never having been observed),[38] but in the Tp series, the stability order is $TpMo(CO)_3R < TpMo(CO)_2(\eta^2\text{-}COR) > TpMo(CO)_3(\sigma\text{-}COR)$. What factors contribute to this reversal in relative stabilities between the two series? This question is addressed in detail later in the theoretical section. Briefly, however, the $Tp(CO)_2Mo$ fragment is strongly hydridized to bond to one addition group to give a six-coordinate structure.[26,29] On the other hand, the diffuse electron cloud of the Cp ligand is ineffective in promoting strong directional character to the frontier orbitals of the $CpMo(CO)_2$ fragment. Consequently, the $CpMo(CO)_2$ fragment may add two groups to give the familiar seven-coordinate, four-legged piano stool complexes, $CpMo(CO)_2L_2$.

The steric bulk of the Tp ligand also promotes six-coordination over seven-coordination. It has been shown that the four "legs" of the piano stool structure of seven-coordinate $TpMo(CO)_3X$ compounds are compressed together.[26] Such compression would favor the migratory CO-insertion reaction which transforms seven-coordinate $TpMo(CO)_3R$ into quasi-six-coordinate $TpMo(CO)_2(\eta^2\text{-}COR)$. Thus, both effects, relief of steric congestion and orbital hybridization, favor the transformation of $TpMo(CO)_3R$ to $TpMo(CO)_2(\eta^2\text{-}COR)$.

Dissociative loss of CO would also be favored by steric compression. As shown in eq 6, the reaction of $LMo(CO)_3^-$ (L = indenyl[39] and Tp[30,40]) with allyl halides gives directly the π-allyl complexes with loss of CO. In contrast, $CpMo(CO)_3^-$ reacts to give the σ-allyl complex which decarbonylates only upon UV irradiation (eq 7).[41] Release of steric congestion may facilitate

$$LMo(CO)_3^- + C_3H_5X \xrightarrow[-CO]{-X^-} LMo(CO)_2(\eta^3\text{-}C_3H_5) \quad (6)$$

(L = indenyl, Tp)

$$CpMo(CO)_3^- + C_3H_5X \xrightarrow{-X^-} CpMo(CO)_3(\eta^1\text{-}C_3H_5) \xrightarrow[-CO]{h\nu} CpMo(CO)_2(\eta^3\text{-}C_3H_5) \quad (7)$$

the decarbonylations in eq 6. However, neither $(\eta^5\text{-indenyl})Mo(CO)_3Me$[39] nor $(\eta^5\text{-}C_5Me_5)Mo(CO)_3Me$[42] has been observed to yield an η^2-acyl complex. Either the steric compression is not sufficient to force alkyl migration and/or electronic factors discourage η^2-acyl formation in these complexes.

The possibility of preparing an η^2-formyl complex according to eq 8a was briefly investigated. It is well-known that CO insertion into M–H bonds to give formyls is often thermodynamically uphill because M–H bonds are generally stronger than metal–alkyl bonds.[43] Given the facility with which alkyl migration occurs in the Tp complexes, it was thought that a similar promotion of the hydride migration might be realized. However, heating $TpMo(CO)_3H$ in THF gave no reaction. At higher temperatures in refluxing DMF or diglyme, a reaction occurred but the product, a tacky glass, appeared to contain the $TpMo(CO)_3^-$ anion. The IR spectrum showed a B–H stretch at 2438 cm^{-1} and C–O stretches at 1880 (s) and 1735 (vs). These bands are close to those observed for $[Et_4N][TpMo(CO)_3]$ in acetonitrile: 2440, 1897 (s), and 1761 (vs). The B–H stretch in particular is informative. In all *neutral* TpMo complexes we have studied, the B–H stretch occurs near 2500 cm^{-1}. Thus, the IR data suggest that $TpMo(CO)_3H$ in DMF or diglyme is merely deprotonated (eq 8b). The enhanced acidity of $TpMo(CO)_3H$ is also a reflection of the stability of the six-coordinate $TpMoL_3$ structure.

$$TpMo(CO)_3H \xrightarrow{\not\rightarrow} TpMo(CO)_2(\eta^2\text{-}COH) \quad (8a)$$

$$TpMo(CO)_3H \xrightarrow{S} [HS_n^+][TpMo(CO)_3^-] \quad (8b)$$

S = DMF or diglyme

Reactions of $TpMo(CO)_2(\eta^2\text{-}COR)$. The addition of nucleophiles, e.g., phosphines, to the η^2-acyl complexes was of interest

(34) King, R. B.; King, A. D., Jr.; Iqbal, M. Z.; Frazier, C. C. *J. Am. Chem. Soc.* **1978**, *100*, 1687.
(35) Butts, S. B.; Strauss, S. H.; Holt, E. M.; Stimson, R. E.; Alcock, N. W.; Shriver, D. F. *J. Am. Chem. Soc.* **1980**, *102*, 5093.
(36) Nesmeyonov, A. N.; Markova, L. G.; Ustynyuk, N. A.; Bogatyreva, L. V. *J. Organomet. Chem.* **1972**, *46*, 105.
(37) McCleverty, J. A.; Wilkinson, G. *J. Chem. Soc.* **1963**, 4096.
(38) A related W complex, $CpW(HCCH)(CO)(\eta^2\text{-}COMe)$, has apparently been prepared, but no structural data are available: Alt, H. G. *J. Organomet. Chem.* **1977**, *127*, 249.
(39) King, R. B.; Bisnette, M. B. *Inorg. Chem.* **1965**, *4*, 475.
(40) Cotton, F. A.; Murillo, C. A.; Stults, B. R. *Inorg. Chim. Acta* **1977**, *22*, 75.
(41) (a) Cousins, M.; Green, M. L. H. *J. Chem. Soc.* **1963**, 889. (b) Piper, T. S.; Wilkinson, G. *J. Inorg. Nucl. Chem.* **1956**, *3*, 104.
(42) King, R. B.; Efraty, A. *J. Am. Chem. Soc.* **1972**, *94*, 3773.
(43) Connor, J. A. *Top. Curr. Chem.* **1977**, *71*, 71.

Table II. Fractional Atomic Coordinates

atoms	X	Y	Z
	(a) $TpMO(CO)_2(\eta^2$-COMe) (**1**)		
MO	0.02577 (7)	0.21059 (5)	0.20983 (4)
C1	0.1240 (11)	0.3181 (7)	0.1474 (7)
C2	0.2264 (9)	0.1915 (6)	0.2908 (5)
C3	0.0782 (9)	0.1356 (7)	0.1031 (6)
C4	0.1387 (11)	0.1332 (8)	0.0174 (6)
O1	0.1856 (11)	0.3798 (6)	0.1147 (6)
O2	0.3442 (7)	0.1826 (7)	0.3398 (5)
O3	0.0324 (7)	0.0593 (4)	0.1382 (4)
B	−0.2940 (9)	0.2755 (6)	0.2694 (5)
N11	−0.0260 (7)	0.3484 (4)	0.2811 (4)
N12	−0.1699 (6)	0.3606 (4)	0.2970 (3)
N21	−0.2154 (6)	0.2299 (5)	0.1236 (4)
N22	−0.3277 (6)	0.2602 (4)	0.1638 (4)
N31	−0.0942 (6)	0.1327 (4)	0.3025 (3)
N32	−0.02271 (6)	0.1718 (4)	0.3151 (4)
C11	0.0558 (9)	0.4342 (6)	0.3184 (5)
C13	−0.0362 (10)	0.4997 (6)	0.3561 (6)
C12	−0.1768 (9)	0.4500 (5)	0.3416 (5)
C21	−0.2780 (9)	0.2227 (6)	0.0343 (5)
C23	−0.4332 (10)	0.2486 (6)	0.0165 (5)
C22	−0.4602 (9)	0.2723 (5)	0.1007 (5)
C31	−0.0660 (9)	0.0446 (6)	0.3529 (5)
C33	−0.1838 (9)	0.0262 (6)	0.3986 (5)
C32	−0.2833 (9)	0.1107 (6)	0.3726 (5)
	(b) $TpMo(CO)_2(\eta^2$-COPh)		
MO	0.20422 (4)	0.19051 (3)	0.39970 (5)
C1	0.0534 (6)	0.0501 (5)	0.2700 (8)
C2	0.2965 (6)	0.1286 (5)	0.1977 (7)
C3	0.0634 (6)	0.2731 (5)	0.3219 (6)
O3	0.1651 (4)	0.3520 (3)	0.3738 (5)
N11	0.4010 (4)	0.2992 (4)	0.5508 (5)
N21	0.1100 (5)	0.2649 (4)	0.6411 (6)
N31	0.2730 (5)	0.0653 (4)	0.4907 (5)
O1	−0.0190 (5)	−0.0329 (4)	0.1906 (7)
O2	0.3482 (5)	0.0896 (5)	0.0792 (6)
C4	−0.0772 (6)	0.2883 (5)	0.2542 (6)
N12	0.4343 (5)	0.3081 (4)	0.7045 (5)
N22	0.1867 (5)	0.2763 (4)	0.7805 (5)
N32	0.3239 (5)	0.1038 (4)	0.6508 (5)
C11	0.5032 (6)	0.3695 (5)	0.5243 (7)
C21	−0.0164 (6)	0.3039 (5)	0.6863 (8)
C31	0.2824 (6)	−0.0525 (5)	0.4157 (8)
C12	0.5554 (6)	0.3827 (5)	0.7728 (8)
C22	0.1088 (7)	0.3202 (5)	0.9110 (7)
C32	0.3635 (6)	0.0179 (5)	0.6777 (8)
C13	0.6049 (6)	0.4252 (5)	0.6641 (7)
C23	−0.0220 (7)	0.3383 (6)	0.8546 (8)
C33	0.3391 (6)	−0.0888 (5)	0.5311 (8)
C5	−0.1017 (6)	0.4024 (5)	0.2858 (7)
C9	−0.1794 (6)	0.1915 (5)	0.1671 (8)
C6	−0.2374 (7)	0.4219 (6)	0.2342 (8)
C8	−0.3128 (7)	0.2114 (6)	0.1098 (8)
C7	−0.3389 (6)	0.3268 (6)	0.1471 (7)
B	0.3364 (7)	0.2355 (6)	0.7729 (8)
	(c) $TpMo(CO)_2[P(OMe)_3](\eta^2$-COMe)		
MO	−0.17182 (5)	0.23124 (3)	0.03330 (6)
P	−0.3480 (2)	0.3256 (1)	0.1115 (2)
C1	−0.0838 (7)	0.3068 (5)	−0.0951 (8)
C2	−0.3602 (7)	0.1906 (4)	−0.1672 (8)
O2	−0.2956 (5)	0.1275 (3)	−0.1935 (6)
N11	−0.2513 (5)	0.1410 (3)	0.1995 (6)
N21	−0.0077 (5)	0.3048 (3)	0.2757 (6)
N31	0.0151 (5)	0.1530 (3)	0.0471 (6)
O1	−0.0220 (7)	0.3563 (4)	−0.1659 (8)
O3	−0.4047 (6)	0.3959 (3)	−0.0017 (7)
O4	−0.5138 (5)	0.2700 (3)	0.1002 (7)
O5	−0.3020 (5)	0.3893 (3)	0.3014 (6)
C3	−0.5111 (9)	0.2000 (6)	−0.287 (1)
C11	−0.3925 (7)	0.0983 (4)	0.1990 (8)
C21	0.0576 (7)	0.3908 (4)	0.3348 (9)
C31	0.0822 (7)	0.1162 (4)	−0.0762 (9)
B	0.0252 (8)	0.1598 (5)	0.3638 (9)
N12	−0.1465 (6)	0.1235 (3)	0.3329 (6)
N22	0.0543 (6)	0.2610 (3)	0.3980 (6)
N32	0.0785 (5)	0.1275 (3)	0.1975 (7)
C4	−0.294 (1)	0.4694 (5)	−0.015 (1)
C5	−0.6393 (9)	0.3123 (5)	0.147 (1)
C6	−0.280 (1)	0.3523 (6)	0.455 (1)
C12	−0.2195 (9)	0.0694 (5)	0.4154 (9)
C22	0.1578 (8)	0.3175 (5)	0.5336 (9)
C32	0.1825 (7)	0.0745 (4)	0.171 (1)
C13	−0.3774 (8)	0.0508 (5)	0.3335 (9)
C23	0.1616 (8)	0.4016 (5)	0.497 (1)
C33	0.1875 (8)	0.0657 (5)	−0.002 (1)
	(d) $TpMo(CO)(PEt_3)(\eta^2$-COMe) (**4**)		
MO	0.4403 (1)	0.0332 (1)	0.20631 (4)
P	0.6313 (3)	0.1484 (2)	0.3448 (1)
B	0.378 (1)	−0.356 (1)	0.1625 (6)
N11	0.6263 (8)	−0.1267 (7)	0.1808 (4)
N21	0.2690 (8)	−0.1323 (7)	0.0990 (4)
N31	0.3134 (8)	−0.1502 (7)	0.2662 (4)
N12	0.5714 (8)	−0.2828 (7)	0.1716 (4)
N22	0.2753 (7)	−0.2863 (7)	0.0911 (4)
N32	0.3099 (8)	−0.3028 (7)	0.2423 (4)
C12	0.703 (1)	−0.360 (1)	0.160 (1)
C22	0.176 (1)	−0.363 (1)	0.019 (1)
C32	0.219 (1)	−0.390 (1)	0.285 (1)
C13	0.848 (1)	−0.248 (1)	0.162 (1)
C23	0.103 (1)	−0.254 (1)	−0.023 (1)
C33	0.163 (1)	−0.291 (1)	0.334 (1)
C11	0.794 (1)	−0.105 (1)	0.1750 (4)
C21	0.165 (1)	−0.113 (1)	0.030 (1)
C31	0.224 (1)	−0.141 (1)	0.3279 (5)
C1	0.275 (1)	0.157 (1)	0.2258 (5)
C2	0.485 (1)	0.165 (1)	0.1190 (5)
C3	0.435 (1)	0.217 (1)	0.037 (1)
O1	0.171 (1)	0.230 (1)	0.2378 (5)
O2	0.6206 (7)	0.2222 (6)	0.1691 (3)
C4	0.854 (1)	0.231 (1)	0.338 (1)
C5	0.662 (1)	0.014 (1)	0.422 (1)
C6	0.560 (1)	0.300 (1)	0.409 (1)
C7	0.979 (1)	0.299 (1)	0.421 (1)
C8	0.748 (2)	−0.119 (1)	0.393 (1)
C9	0.572 (2)	0.449 (1)	0.370 (1)

since the reaction could displace either the oxygen of the η^2-acyl group (eq 9a) or a carbonyl (eq 9b). With both $P(OMe)_3$ and

$$TpMo(CO)_2(\eta^2\text{-COMe}) + PR_3 \rightarrow \begin{cases} TpMo(CO)_2L(\eta^1\text{-COR}) & (9a) \\ TpMo(CO)L(\eta^2\text{-COR}) + CO & (9b) \end{cases}$$

3, L = $P(OMe)_3$ (55%)
4, L = PEt_3 (74%)

PEt_3, the reaction follows the course shown in eq 9b. The identity of the products was established by ^1H and ^{13}C NMR, by IR and mass spectrometry, and by single-crystal structure determinations.

The trimethylphosphite adduct, **3**, is the sole product of the reaction. Adduct **3** has a single ν_{CO} stretch at 1800 cm^{-1}, and the acyl CO stretch occurs at 1508 cm^{-1}. The pz rings are all nonequivalent in both the ^1H and ^{13}C NMR spectra. The acyl and carbonyl carbons both appear as doublets at δ 267.6 ($^2J_{PC}$ = 48 Hz) and δ 236.4 ($^2J_{PC}$ = 14 Hz), respectively. The molecule possesses no symmetry. It was, therefore, not possible to determine if the η^2-COMe group was fluxional as it was in the parent dicarbonyl, **1**, since the three pz rings are nonequivalent in any event.

The reaction of **1** with PEt_3 gave, in addition to a 74% yield of the adduct **4**, a 12% yield of the triply bonded dimer,

Table III. Selected Bond Distances for Compounds **1–4**[a,e]

	1	2	3	4	av
Mo–C_a	2.018 (8)	2.021 (5)	2.003 (6)	2.002 (8)	2.01 [1]
Mo–O_a	2.222 (5)	2.189 (3)	2.200 (4)	2.246 (5)	2.21 [3]
C_a–O_a	1.23 (1)	1.224 (6)	1.224 (8)	1.239 (9)	1.23 [1]
Mo–CO	1.988 (9)	2.029 (6)	1.896 (7)	1.898 (8)	1.95 [5]
C–O	1.14 (1)[c]	1.13 (1)[c]	1.183 (8)	1.179 (9)	1.16 [3]
Mo–L[b]	1.932 (8)	1.946 (6)	2.416 (2)	2.517 (2)	
Mo–N_C	2.194 (6)	2.205 (4)	2.250 (5)	2.277 (6)	2.24 [3][d]
Mo–N_L	2.255 (6)	2.250 (4)	2.194 (5)	2.249 (6)	2.22 [4][d]
Mo–N_A	2.170 (5)	2.180 (4)	2.199 (5)	2.203 (6)	2.19 [2]

[a] Standard deviations obtained from the least-squares refinements are enclosed in parentheses, while those calculated for more than one value with the formula $\sigma = \{\sum(x - \bar{x})^2/(N-1)\}^{1/2}$ are enclosed in brackets. [b] L = C(2)O(2) for **1** and **2**, $P(OMe)_3$ for **3**, and PEt_3 for **4**. [c] Average of the two values for C(1)–O(1) and C(2)–O(2). [d] Mo–N_C average includes the two Mo–N_L values for **1** annd **2** (L = CO); Mo–N_L average includes only the two values for **3** and **4**. [e] In this and the following table, the atom labeling is referred to the figure below (also see text).

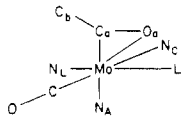

Table IV. Selected Bond Angles for **1–4**[a]

angle	1	2	3	4	av
O_a–C_a–C_b	125.2 (8)	122.6 (5)	122.8 (6)	123.5 (7)	124 [1]
O_a–C_a–Mo	82.6 (5)	80.8 (3)	82.2 (4)	84.2 (5)	82 [1]
Mo–C_a–C_b	152.3 (7)	156.5 (4)	154.9 (6)	152.2 (6)	154 [2]
C_a–O_a–Mo	64.2 (4)	65.7 (3)	64.4 (4)	62.5 (4)	64 [1]
C_a–Mo–O_a	33.2 (3)	33.5 (2)	33.4 (2)	33.3 (2)	33.4 [1]
N_L–Mo–C_a	88.5 (3)	86.8 (2)	117.4 (2)	84.2 (3)	
N_L–Mo–O_a	87.3 (2)	87.8 (2)	84.2 (2)	114.5 (2)	
N_L–Mo–N_C	82.0 (2)	82.5 (2)	81.7 (2)	81.1 (2)	81.8 [6]
N_L–Mo–L	176.0 (3)	176.8 (3)	162.8 (1)	163.5 (2)	
N_L–Mo–C	97.4 (3)	100.1 (2)	98.5 (2)	96.3 (3)	98 [2]
N_L–Mo–N_A	84.4 (2)	82.5 (2)	79.8 (2)	76.2 (2)	
N_C–Mo–C_a	122.2 (3)	117.4 (2)	95.4 (2)	96.0 (3)	
N_C–Mo–O_a	89.1 (2)	84.4 (2)	87.0 (2)	87.4 (2)	87 [2]
N_C–Mo–L	94.1 (3)	94.4 (2)	89.0 (1)	90.6 (2)	92 [3]
N_C–Mo–C	162.9 (3)	162.0 (2)	174.2 (3)	176.8 (2)	
N_C–Mo–N_A	82.0 (2)	81.8 (2)	85.5 (2)	87.0 (2)	84 [3]
L–Mo–C_a	94.4 (3)	95.6 (2)	77.6 (2)	111.0 (2)	
L–Mo–O_a	93.7 (3)	92.9 (2)	109.8 (1)	79.0 (2)	
L–Mo–C	86.0 (4)	82.5 (2)	94.8 (2)	91.5 (2)	
L–Mo–N_a	94.1 (3)	94.4 (2)	86.1 (1)	89.2 (2)	91 [4]
C–Mo–C_a	74.9 (4)	74.9 (4)	89.8 (3)	85.4 (3)	
C–Mo–O_a	108.0 (3)	113.4 (2)	95.8 (2)	95.3 (3)	
C–Mo–N_A	80.9 (3)	80.9 (2)	90.4 (2)	90.7 (3)	
n_A–Mo–C_a	153.7 (3)	156.6 (2)	162.7 (2)	159.5 (3)	158 [4]
N_A–Mo–O_a	168.6 (2)	164.1 (2)	163.2 (2)	166.9 (2)	166 [2]
θ_1[b]	117.6	117.7	131.5	137.2	
θ_2[b]	122.5	121.2	112.5	108.9	
θ_3[b]	119.9	121.0	116.0	113.4	

[a] Labeling for the atoms in the inner coordination sphere is derived from the figure in Table III. [b] Angles between the planes of the pyrazole rings containing the nitrogens, N_A, N_L, N_C: $\theta_1 = \angle N_A N_C$, $\theta_2 = \angle N_A N_L$, $\theta_3 = \angle N_L N_C$.

$Tp_2Mo_2(CO)_4$.[28] The mechanism whereby the latter is formed is not known.

The CO-stretching frequency, 1765 cm^{-1}, of **4** is 35 cm^{-1} lower than that of **3**. This decrease is as expected since the PEt_3 group is more electron donating than $P(OMe)_3$. However, the acyl C-O-stretching frequencies of both **3** and **4** are virtually identical (1510 vs. 1508 cm^{-1}).

In contrast to the doublets observed for the acyl and CO carbons of **3**, these groups gave singlets at 253.6 and 201.3, respectively, in adduct **4**. The difference in these spectral properties led us to suspect that **3** and **4** might have different structures. Accordingly, the structures of both **3** and **4** were determined by X-ray diffraction. The only major difference was the orientation of the acyl group with respect to phosphine ligand. Both **3** and **4** have the acyl C–O bond aligned more or less along a P–Mo–N vector, but **3** has the carbon adjacent to N while **4** has the carbon adjacent to P (see Figures 3 and 4). The orientational preference of the η^2-acyl group is discussed later in the theoretical section.

A few other reactions of the acyl complex **1** have been examined briefly. Complex **1** failed to react with trifluoroacetic acid or $[Me_3O][BF_4]$. Its reaction with I_2 produced $TpMo(CO)_3I$. The fate of the acetyl group was not established. With HCl (aqueous) in acetonitrile, **1** formed an insoluble, brick-red product (ν_{CO} (KBr) 2036 (w), 1914 (m), 1802 (m)) which could not be adequately characterized. With MeLi, **1** reacted to give a complex mixture from which pure solids could not be extracted. However, treatment of the mixture with Me_3O^+ regenerated **1**, which suggests that the Me group of the acyl ligand was deprotonated by MeLi and reprotonated by the oxonium cation. Deprotonations of both η^2- and η^1-acetyl metal complexes have recently been reported.[44,45]

X-ray Structure Determinations of 1–4. The structures of **1–4** are depicted in Figures 1–4. The numbering schemes in these figures correspond to the atomic positions (Table II) and the complete tables of bond distances and angles as found in the supplementary material. For easy comparisons, the simplified atom labeling scheme for the inner coordination sphere shown in Table III will be used in all subsequent discussion. In the simplified scheme, C_a and O_a refer to the acyl carbon and oxygen, C_b is the carbon of the Me or Ph bonded to C_a, and N_A, N_L, and N_C are the Tp nitrogen donors trans to the acyl, ligand L, and C(1)O(1), respectively. In **1** and **2**, L = C(2)O(2), in **3**, L = $P(OMe)_3$, and in **4**, L = PEt_3. In all cases, C(1)O(1) will be referred to as simply CO.

All the compounds, **1–4**, may be viewed as slightly distorted octahedral structures in which the η^2-acyl group occupies one coordination site. The intraligand bond distances and angles in the coordinated Tp, $P(OMe)_3$, and PEt_3 groups are unexceptional and will not be discussed further. However, the effect of substitution of a carbonyl with a bulky $P(OMe)_3$ or PEt_3 group might be noted. In **1** and **2**, the angles, θ_1–θ_3 (Table IV), between the planes of the pyrazole rings of the Tp ligand are very close to 120°. In **3** and **4**, however, the angle θ_1 opens to 132 and 138°, respectively, with concomitant decreases in the remaining two angles, θ_2 and θ_3. These changes in θ are clearly in response to the increased cone angles[47] of the $P(OMe)_3$ (107°) or PEt_3 (132°) ligands.

Within the inner coordination sphere, the Mo–N distances show some interesting variations (Table III). In general, the Mo–N_A bond is the shortest Mo–N bond in these molecules, the only exception being Mo–N_L (2.19) and Mo–N_A (2.20) in **3**. The longest Mo–N bonds are those trans to the carbonyls (av 2.24), and those trans to P fall in between. On the basis of these Mo–N distances, the following order of the trans influence is deduced: CO > PEt_3 > η^2-COR ~ $P(OMe)_3$.

The Mo–CO and C–O distances reflect the relative electron densities on Mo in this series of compounds. Substitution of carbonyl by PR_3 increases the electron density on the metal which, in turn, leads to increased π-back-bonding to the remaining carbonyl. This effect is reflected by the average ν_{CO} frequencies (Table V) for **1–4**: 1920, 1916, 1800, and 1765 cm^{-1}. The Mo–CO distances for **1** and **2** average 1.97 [4], while those for **3** and **4** are shorter (1.90 [1]). The C–O bond lengths show the opposite trend: 1.14 [1] for **1** and **2**, and 1.18 [1] for **3** and **4**. Thus, as the availability of metal electrons increases, the Mo–C distances shrink and the C–O distances increase in accordance with the relative importance of the valence bond resonance structures, M—C≡O ↔ M=C=O.

(44) Ho, S. C. H.; Straus, D. A.; Armantrout, J.; Schaefer, W. P.; Grubbs, R. H. *J. Am. Chem. Soc.* **1984**, *106*, 2210.
(45) (a) Baird, G. J.; Davies, S. G. *J. Organomet. Chem.* **1983**, *248*, C1. (b) Aktogu, N.; Felkin, H.; Davies, S. G. *J. Chem. Soc., Chem. Commun.* **1982**, 1303.
(46) Fagan, P. J.; Manriquez, J. M.; Marks, T. J.; Day, V. W.; Vollmer, S. H.; Day, C. S. *J. Am. Chem. Soc.* **1980**, *102*, 5393.
(47) Tolman, C. A. *J. Am. Chem. Soc.* **1970**, *92*, 2956.

Table V. Comparison of Structral and IR Features of η^2-Acyl Complexes

	d(M–C_a), Å	Δ,[a] Å	acyl d(C–O), Å	acyl ν_{CO}	ν_{CO}	ω[b]	ref
$RuL_2I(CO)(COMe)$[d]	1.92	0.44	1.21	1599	1907		25
$MoL_3Cl(CO)(COR)$[d]	2.02	0.30	1.23	1500	1810	27	22a
$Tp^*Mo(CO)_2(COPh)$	2.00	0.29	1.24	na	na	na	23
$Tp^*Mo(CO)_2(COC_6H_{11})$	2.00	0.29	1.27	na	na	na	23
$[Mo(\mu\text{-}Cl)(CO)_2L(COR)]_2$[d]	2.02	0.27	1.22	1585	1882[c]	32	21
$[W(\mu\text{-}Cl)(CO)_2L(COR)]_2$[d]	2.03	0.26	1.23	1530	1872[c]	32	22b
4	2.00	0.25	1.24	1510	1765	69	this work
$V(dppe)(CO)_3(COR)$	2.01	0.23	1.20	1500	1862[c]	~45	24
3	2.00	0.20	1.22	1508	1800	~77	this work
1	2.02	0.20	1.23	1510	1920[c]	11	this work
2	2.02	0.17	1.22	1490	1916[c]	20	this work
$Cp_2TiCl(COMe)$	2.07	0.12	1.18	1620			1b
$Cp_2ZrMe(COMe)$	2.20	0.09	1.21	1540			1a
$Cp_2^*ThCl(COR)$	2.44	−0.07	1.18	1469			46

[a] $\Delta = d(M\text{–}O) - d(M\text{–}C)$ for the acyl group. [b] Angle defining the orientation of the η^2-COR group with respect to the ML_5 fragment—see text. [c] Average of all the IR-stretching frequencies of the terminal CO groups. [d] L = PMe_3.

In contrast, it is difficult to find any internally consistent set of structural changes in the η^2-acyl portion of these structures which can be ascribed to increased back-bonding to the η^2-acyl group. If the two resonance extremes, are considered, an increase of electron density might favor B over A and result in a shorter Mo–C_a bond length. Indeed, the two P-substituted compounds,

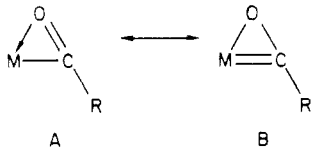

A B

3 and **4**, do show a slight contraction of the Mo–C_a bond (2.00 [1] for **3** and **4** vs. 2.02 [1] for **1** and **2**), but the contraction is within 3σ of the difference. An increase in the contribution of B should increase the C_a–O_a bond length, but the C_a–O_a bond length is the same in all four compounds, **1**–**4**, within experimental error. There is too much scatter in the Mo–O_a values to draw any generalizations from these data, although one might expect that the Mo–A_a distance would increase as the electron density on the metal increased.

At this point, we should point out that the Mo–C distances in general show a very good correlation with formal bond order. Mo—C single bonds show a range of values, 2.29–2.36 Å,[48] Mo=C (carbene) lengths fall in the range 1.95–2.15 Å,[49] and Mo≡C (carbyne) triple bond distances span the values 1.80–1.84 Å.[50] Furthermore, these distances are very close to the sum of the appropriate atomic radii. The radii for singly, doubly, and triply bonded Mo may be taken as one-half the observed Mo—Mo, Mo=Mo, and Mo≡Mo distances in $Cp_2Mo_2(CO)_6$,[51] $Cp_2Mo_2(CO)_4(\mu\text{-}C_{13}H_8)$,[52] and $Cp_2Mo_2(CO)_4$,[53] respectively. The resulting values, 1.62, 1.40, and 1.22 Å, when added to the radii for singly, doubly, or triply bonded carbon give values of 2.39, 2.07, and 1.82 Å as the calculated distances for Mo—C, Mo=C, and Mo≡C bonds. The agreement between the observed distances and these sums of the radii is excellent. Thus, the observed Mo–C_a distances (av 2.01 Å) suggest significant double bond character for this bond. The EHMO results (see below) are in accord with this observation.

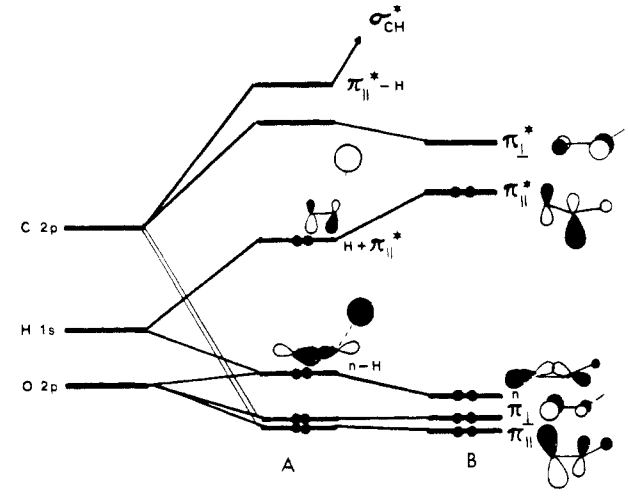

Figure 5. (A) Molecular orbitals of an (H)(CO) molecular fragment with the H and CO groups positioned to bond to a four-legged piano stool structure, e.g., $CpMo(CO)_2$. (B) Fragment molecular orbitals appropriate for an η^2-HCO group.

The parameter, $\Delta = d(Mo\text{–}O_a) - d(Mo\text{–}C_a)$, has been used as a gauge of the strength of the dihapto nature of η^2-acyl complexes. Table V lists all the transition-metal η^2-acyls which have been structurally characterized plus one actinide structure. The compounds are arranged vertically in order of decreasing Δ. As these data show, there are no correlations at all between any of the sets of parameters, Δ, d(M–C_a), $\nu_{C_aO_a}$, ν_{CO}, or $d(C_a - O_a)$. The C_a–O_a distances vary irregularly between 1.18 and 1.27 Å, while Δ varies from 0.44 to −0.07 Å. For the six-coordinate, d^4 complexes of V, Mo, and W, the M–C_a distance is essentially invariant at 2.01 ± 0.01 Å.

In the d^4, $L_5M(\eta^2\text{-COR})$ series, an orientiational preference for the η^2-acyl group is evident. C defines ω for the dicarbonyl complexes, and D defines ω for **3** and **4** (the view is down the z axis; the remaining ligand trans to the η^2-acyl group is not shown).

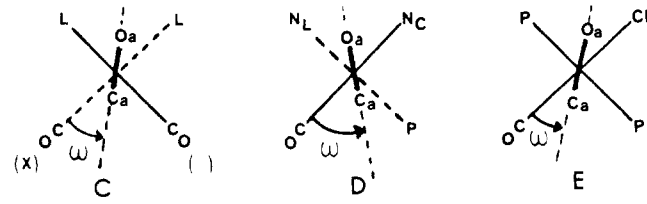

All the dicarbonyl complexes listed in Table V have values of ω between 11° and 45°, which places C_a above the quadrant between the two cis carbonyls. In the PEt_3-substituted complex, **4**, the C_a–O_a group lines up nearly parallel to the P–Mo–N axis with C_a adjacent to P. The value of ω is 69°. In the $P(OMe)_3$ complex, the η^2-acyl group is again more or less aligned along the P–Mo–N

(48) (a) Churchill, M. R.; Fennessey, J. P. *Inorg. Chem.* **1967**, *6*, 1213. (b) Arigaratue, J. P.; Bierrum, A. M.; Green, M. L. H.; Ishaq, M.; Prout, C. K.; Swanwick, M. G. *J. Chem. Soc. A* **1969**, 1309.

(49) (a) Messerle, L.; Curtis, M. D. *J. Am. Chem. Soc.* **1982**, *104*, 889. (b) Fischer, E. O.; Hoefelder, H.; Friedrich, P.; Kreisl, F. R.; Hutner, G. *Chem. Ber.* **1977**, *110*, 3467. (c) Green, M.; Norman, N. C.; Orpen, A. G. *J. Am. Chem. Soc.* **1981**, *103*, 1267.

(50) (a) Fischer, E. O.; Lindner, T. L.; Frank, A.; Fritz, R. K. *Angew. Chem., Int. Ed. Engl.* **1976**, *15*, 157. (b) Green, M.; Orpen, A. G.; Williams, I. D. *J. Chem. Soc., Chem. Commun.* **1982**, 493. (c) Botrill, M.; Green, M. *J. Am. Chem. Soc.* **1979**, *99*, 5795.

(51) Adams, R. D.; Collins, D. M.; Cotton, F. A. *Inorg. Chem.* **1974**, *13*, 1086.

(52) D'Errico, J. J.; Curtis, M. D. *J. Am. Chem. Soc.* **1983**, *105*, 4479.

(53) Klingler, R. J.; Butler, W. M.; Curtis, M. D. *J. Am. Chem. Soc.* **1978**, *100*, 5034.

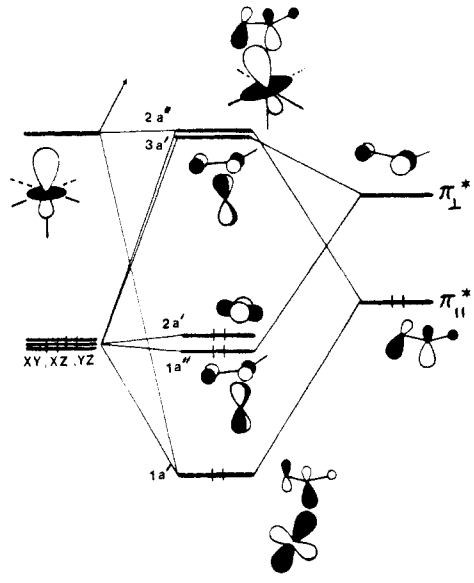

Figure 6. MO energy diagram for $H_5Mo(\eta^2\text{-}HCO)^{4-}$ showing the interaction of the H_5Mo^{3-} and HCO^{1-} fragments.

axis, but in this case C_a is adjacent to N and $\omega = -77°$. E defines ω for the $M(PMe_3)_3Cl(CO)(\eta^2\text{-}COR)$ complexes. In these latter complexes, $\omega = 32°$. The electronic origin of this orientational preference of the η^2-acyl group is discussed in the following sections.

EHMO Calculations[54]

Bonding of η^2-HCO to the Metal. The orbitals of the HCO^{-1} fragment are shown in Figure 5B. The three, *lowest energy orbitals*, $\pi_\parallel$, $\pi_\perp$ and n, are not much perturbed by bonding to the L_5M fragment and will be ignored in the subsequent discussion. The HOMO of the HCO^{1-} fragment is $\pi_\parallel$*. This orbital is C—O antibonding, C–H bonding, and largely localized on the C as shown by the reduced charges: 1.43 (C), 0.46 (O), and 0.11 (H). The p orbital on the carbon is also hybridized with C(2s) as shown in the figure. Thus, the donor properties of the HOMO are maximized by binding the Lewis acid site to the carbon end of the HCO^{1-} fragment.

The LUMO of the HCO^{1-} fragment is $\pi_\perp$*, also largely localized on the carbon atom (reduced charges: 1.62 (C) and 0.38 (O)). It is the LUMO which acts as the π-acceptor in η^2-acyl complexes of transition metals.

Figure 6 shows the MO energy diagram for the bonding of the η^2-HCO^{1-} fragment to a H_5Mo^{3-} fragment. This model is chosen to present the salient features of the bonding in the absence of any complicating factors, e.g., π-bonding to ancillary ligands on the metal center. The orbitals of the H_5Mo^{3-} fragment are the now familiar z^2 hybrid above the "t_{2g}" set.[55] The x^2–y^2 orbital is at high energy and does not participate in bonding to the η^2-acyl fragment. In Figure 6, the orientation of the acyl group corresponds to $\omega = 45°$ (see above).

From an energetic viewpoint, the greatest contribution to the bonding is provided by the interaction of $\pi_\parallel$* with the z^2 hybrid and with the $(xz + yz)$ orbitals. Thus, in the resultant MO, z^2 and $(xz + yz)$ are mixed so as to maximize the bonding overlap with C_a and minimize the antibonding overlap with O_a (see Figure 6).

The $(xz - yz)$ hybrid interacts with $\pi_\perp$* and is slightly stabilized. This is the π-back-bonding component of the metal–η^2-acyl interaction. Note that there is also a M–O_a antibonding overlap. Mixing x^2–y^2 into the $(xz - yz)$ hybrid could tilt the latter and maximize bonding overlap with C_a and minimize antibonding overlap with O_a. However, such a rehybridization is precluded because the x^2–y^2 orbital has been displaced to high energy by its σ* interaction with the hydride ligands. In the $\omega = 0.0°$ rotamer, however, the xy orbital can and does mix effectively with the yz orbital to form the tilted hybrid shown below.

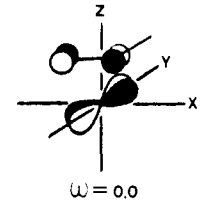

$\omega = 0.0$

We can dissect the bonding further. A fragment MO (FMO) analysis shows that MO's derived from $\pi_\perp$* contain 0.42e. Since $\pi_\perp$* had no electrons to start with, 0.42e is the extent of back-donation from Mo to the HCO^{1-} fragment and represents substantial double bond character in the Mo–C_a bond.

The Mulliken overlap population analysis and the reduced energy matrix show a surprising result. These matrices are shown below. A positive overlap population corresponds to net bonding

	C	O	H
Mo	0.58	0.03	-0.03
C		0.91	0.82
O			-0.05

overlap population

	C	O	H
Mo	-12.07	-0.62	+0.61
C		-30.53	-21.57
O			+1.44

energy matrix

between the atoms, and a negative population represents an antibonding interaction. The reduced energy matrix shows a particular bond's contribution to the total energy of the molecule. A negative value corresponds to stabilization (bonding) and vice versa.

The surprising feature is the very low contribution the Mo–O bond makes to the electronic energy of the molecule. The low Mo–O_a overlap population is a result of the fact that Mo–C_a *atomic* overlaps dominate the (H_5Mo)–(HCO) *group* overlaps. Thus, when $\pi_\parallel$* or $\pi_\perp$* form bonding combinations with metal orbitals, the Mo–C_a atomic overlaps are bonding, but the Mo–O_a overlaps are antibonding since the C_a and O_a atomic orbitals are out of phase in the $\pi_\parallel$* and $\pi_\perp$* FMO's. This effect is easily seen in the orbital drawings above and in Figure 6.

Rotational Preference of the η^2-HCO Group. In the H_5Mo^{3-} fragment, the z^2 hybrid is symmetric about the z axis and thus does not contribute to any electronic barriers to rotation of the η^2-HCO group. The xz and yz orbitals are degenerate and can be rehybridized to give any desired orientation to the metal d_π orbital used in back-bonding. Thus, one expects and finds only a small barrier to rotation of the HCO group about the z axis. The $\omega = 0.0°$ conformation is calculated to be 1.9 kcal/mol more stable than the $\omega = 45°$ rotamer due to the mixing of yz and xy (discussed above) which gives better overlap with $\pi_\perp$*.

The situation is quite different for $(HCN)_3(CO)_2Mo(\eta^2\text{-}HCO)^{1+}$. EHMO calculations were performed on this molecule as a model for the $Tp(CO)_2Mo(\eta^2\text{-}HCO)$ complexes. In the "undistorted" model, all intraligand angles in the $(HCN)_3(CO)_2Mo$ fragment were set at 90° or 180°; i.e., all ligands lay on the $\pm x$ or $\pm y$ axis The FMO's of the $(HCN)_3(CO)_2Mo^{2+}$ fragment have been discussed fully elsewhere.[56] The major difference of interest between the $(HCN)_3(CO)_2Mo$ and H_5Mo fragments is that in the former, the z^2 hybrid and the $(xz + yz)$ orbital mix through the agency of the carbonyl groups to give the hybrids shown below.

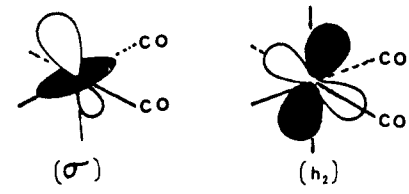

(σ) (h_2)

(54) EHMO calculations have been reported recently for compounds of the type, $Cp_2M(\eta^2\text{-}COR)X$: Tatsumi, K.; Nakamura, A.; Hoffman, P.; Stauffert, P.; Hoffmann, R. *J. Am. Chem. Soc.* **1985**, *107*, 4440.

(55) (a) Elian, M.; Hoffmann, R. *Inorg. Chem.* **1975**, *14*, 1058. (b) Hoffmann, R. *Angew. Chem., Int. Ed. Engl.* **1982**, *21*, 711.

(56) Curtis, M. D.; Eisenstein, O. *Organometallics* **1984**, *3*, 887.

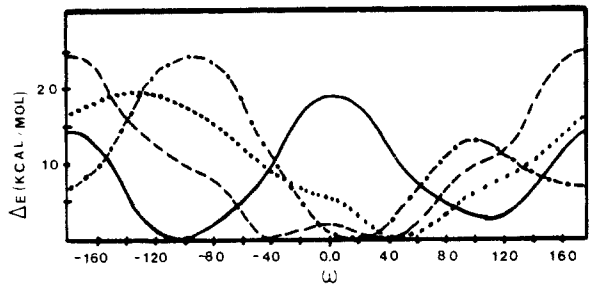

Figure 7. Energy profiles computed by the EHMO method for rotation of the η^2-HCO group about its axis of bonding to the metal: (A) (···) undistorted $(HCN)_3(CO)_2Mo(\eta^2\text{-}HCO)^+$; (B) (-·-) distorted $(HCN)_3(CO)_2Mo(\eta^2\text{-}HCO)^+$ (structure C); (C) (—) $(HCN)_3(CO)(PH_3)Mo(\eta^2\text{-}HCO)^+$ with bending distortion (structure D); (D) (- - -) $(H_3P)_3(CO)ClMo(\eta^2\text{-}HCO)$ with no bending distortion (structure E). See text and figures for definition of ω.

The $(xz + yz) + \lambda z^2$ hybrid, h_2, now points out between the carbonyls and is no longer degenerate with $(xz - yz)$. Consequently, the overlap of $\pi_\parallel^*$ with h_2 is much better in the $\omega = 45°$ conformation than in any other rotomeric configuration: $\langle \pi_\parallel^* | h_2 \rangle = 0.192$ ($\omega = 45°$) and 0.100 ($\omega = 225°$). The better overlap at $\omega = 45°$ leads to a stabilization of the bonding combination 1a′ (Figure 6). The computed energy as a function of ω is shown in Figure 7A. There is a flat minimum symmetric about $\omega = 45°$. The maximum energy (+19.1 kcal/mol) occurs 180° away ($\omega = 225° = -135°$).

Of the five complexes in Table V which have cis $(CO)_2$ groups and for which the data are available, only one, V(dppe)$(CO)_3$(COR), has $\omega \approx 45°$. Is our calculational model wrong, or are there other factors at work which influence the equilibrium geometry of these η^2-acyl complexes? At this point, we noticed that the compounds, **1–4**, all had a distortion: one set of trans ligands is depressed down out of the *xy* plane away from the η^2-acyl group (see Table IV). For example, in **1** and **2**, the angles N_C–Mo–C are 162.9 (3)° and 162.0 (2)°, whereas the angles N_L–Mo–L (L = C(2)–O(2)) are closer to the ideal 180°, vis., 176.0 (3)° and 176.8 (3)°. These distortions are indicated by dashed lines in C and D. The depression of *one* set of trans ligands introduces additional asymmetry into the potential field which could cause the minimum to shift from $\omega = 45°$ calculated for the symmetric model. (In the V complex in Table V, *both* sets of trans P–V–CO angles are depressed to ~165°, thereby maintaining C_s symmetry in the potential field of the $VP_2(CO)_3$ fragment.)

The potential energy curve calculated for an $(HCN)_3(CO)_2Mo(\eta^2\text{-}HCO)$ model which incorporates the distortion indicated in C is shown in Figure 7B. The well now has a broad minimum centered at $\omega = 15°$. There is a second minimum in the curve near $\omega = 170°$, which is about 7.5 kcal/mol higher in energy. Two barriers of 24 kcal/mol ($\omega = -100°$) and 13 kcal/mol ($\omega = +100°$) separate the two minima.

We conclude that there is a moderately strong electronic preference for the η^2-acyl group in these distorted structures to adopt a rotational conformation with ω near 15°. The flatness of the curve in the region of the minimum would allow considerable amplitude in the librational motion of the η^2-acyl about the *z* axis. The observed values of ω for **1** and **2** are 11° and 20°, respectively, both values being well within the flat portion of the computed energy well. A large librational amplitude in ω, coupled with an e symmetry bending mode of the four ligands in the *xy* plane, is sufficient to give the observed fluxional averaging of the structures of **1** and **2** (see above).

How does the bending down of two ligands shift the energy minimum toward lower values of ω, i.e., toward the depressed bonds, and why is there a distortion in the first place? The effect of the bending distortion is most clearly seen by returning to the H_5Mo^{3-} fragment. If all the H atoms lie on the axes, then the metal p and d_π orbitals are orthogonal and do not mix. When one set of trans H atoms is moved off of, say, the *x* axis, then the p_x and d_{xz} orbitals are mixed as shown in Scheme II.

The resulting p_x–*xz* hybrid points up toward the η^2-acyl ligand

Scheme II

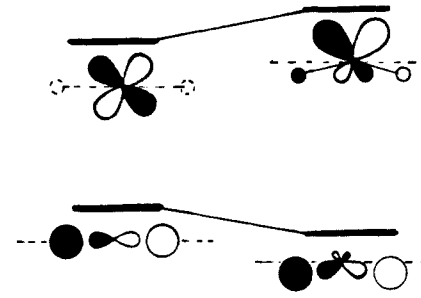

and the overlap between $\pi_\parallel^*$ and the p–d hybrid ($S = 0.20$) is larger than between $\pi_\parallel^*$ and a pure *xz* orbital ($S = 0.17$). Thus, the acyl group lines up with the depressed bonds ($\omega = 0.0°$). For the $H_5Mo(\eta^2\text{-}HCO)^{4-}$ model, the $\omega = 0.0°$ orientation is calculated to be 13.4 kcal/mol more stable than the $\omega = 90°$ orientation in which the acyl group lines up over the undistorted H–M–H bonds. Furthermore, the total energy of the distorted molecule is lower than the undistorted one by 10.5 kcal/mol. Similar decreases in total energies were noted for the other molecules studied.

Thus, there is an inherent tendency in these $L_5Mo(\eta^2\text{-acyl})$ structures toward a deformation which bends one or more pairs of transoid ligands away from the acyl group. The acyl group tends to align itself parallel to the depressed bonds. If there exists electronic asymmetry such as that in the $L_3(CO)_2Mo$ fragments, discussed above, then the two effects work in concert to set the energy minimum at $0° < \omega < 45°$.

The dimers, $[M(\eta\text{-}Cl)(CO)_2L(COR)]_2$, listed in Table V also show this type of bending distortion. The Cl–M–CO angles may be separated into two sets with values of ca. 166° and 175°. Although no calculations on these specific compounds were performed, their potential energy curves for acyl rotation would undoubtedly resemble that in Figure 7B. Their values of ω (32°) are near the bottom of this energy well.

With these results in hand, the orientation of the η^2-acyl group in the PR_3-substituted compounds, **3** and **4**, can be understood. In these compounds, the N–Mo–P bonds are bent back: $\angle N_L$–Mo–L = 162.8 (1)° and 163.5 (2)° (Table IV). The acyl group will therefore tend to line up over these bonds. The angle, ω, is defined in D above. Figure 7C shows the computed potential curve. There are two minima, one at $\omega = -105°$ and one at $\omega = +110°$. The latter is about 3 kcal/mol higher in energy than the former. In one ($\omega = -105°$), the carbon end of the acyl group lies over the Mo–N bond. In the other minimum ($\omega = +110°$), the carbon lies over the Mo–P bond. Just by chance, we have structurally characterized molecules trapped in each minimum (cf. Figures 3 and 4).

The absolute values of ω for **3** (-77°) and **4** (+69°) do not correspond very well with the values of ω computed for the minima in Figure 7C. However, the bottoms of the energy wells are so flat that the computed energy of the $\omega = -77°$ and +69° conformations are only about 5 kcal/mol higher than the bottoms of the computed potential wells in the model compounds.

For the sake of completeness, a potential energy curve for $MoL_3Cl(CO)(\eta^2\text{-}COR)$ was computed (Figure 7D, ω is defined in E above). There is an extremely broad minimum with a small (<2 kcal/mol) hump in the middle where the acyl group crosses the Mo–CO bond. The bottom of the well is at $\omega = 40°$. The observed value is 27°.

In summary, the calculations show that there are preferred rotational orientations of the η^2-acyl group in $L_n(CO)_{5-n}M(\eta^2\text{-acyl})$ complexes. There is also an inherent tendency in these complexes to exhibit a bending deformation (essentially a second-order Jahn–Teller distortion) such that one or both pairs of trans ligands in the plane adjacent to the η^2-acyl group bend away from that group. The preferred orientation of the acyl group is to be aligned along the depressed pair of bonds and/or with the carbon of the acyl group adjacent to a carbonyl.

η^1- vs. η^2-Acyl Structures. It was shown in the previous discussion that the Mo–(η^2-HCO) interaction results in a very weak

Chart I

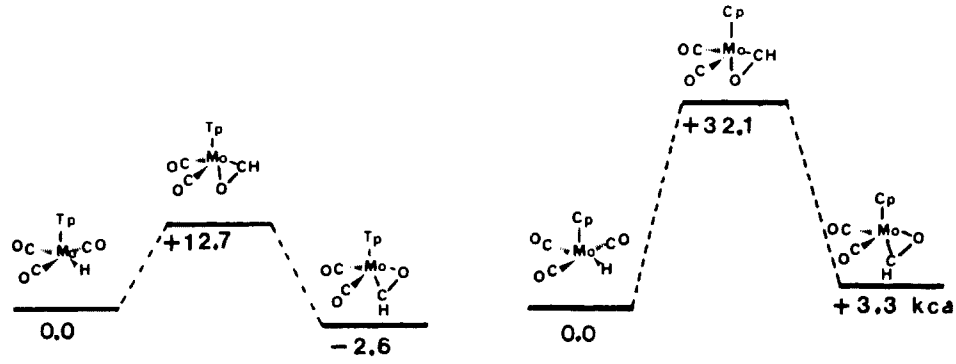

Table VI. Mulliken Overlap Populations for Selected Bonds in $L_3(CO)_2Mo(H)(CO)^{n+}$ and $L_3(CO)_2Mo(\eta^2\text{-HCO})^{n+}$ (L_3 = $(HCN)_3$, n = 1; L_3 = Cp, n = 0)

compd	L_3	Mo–C	C–O	Mo–H	C–H	Σ	Δ	ΔΔ
(H)(CO)	$(HCN)_3$	0.71	1.19	0.47	0.04	2.41		
							0.16	
(η^2-HCO)	$(HCN)_3$	0.52	0.94	−0.03	0.82	2.25		
								0.07
(H)(CO)	Cp	0.71	1.17	0.44	0.06	2.39		
							0.23	
(η^2-HCO)	Cp	0.43	0.93	−0.03	0.83	2.16		

Mo–O_a bond. What, then, is the role of the Mo–O_a interaction in stabilizing the η^2-acyl structure? Figure 8 shows the MO energy level diagram for $(HCN)_3(CO)_2Mo(CHO)^{1+}$ complexes in which the geometry of the HCO fragment was varied from that of the η^2 structure (Figure 8A), through an intermediate (Figure 8B), to an η^1-CHO (Figure 8C) complex. The differences in total energies (ΔE) for the given electron configurations are shown also in the figure.

It is surprising at first glance to see that the total energy increases by only +3.09 kcal/mol when the oxygen is detached from the molybdenum. There are two reasons why the energy changes so little. First, as shown above, there is not much of a bond between Mo and O_a to start with. The Mo–O_a overlap population is only 0.04 in the η^2-acyl structure, so not much is lost when the bond is broken.

The second reason for the small ΔE is the greatly improved Mo–C_a bonding in the η^1 structure compared to the η^2. An intended crossing of the 1a′ and 3a′ levels is not explicitly shown in Figure 8, but in the η^2 structure, 1a′ is mostly ($xz + yz$) and 3a′ is ca. 50% z^2. As the acyl group moves from η^2 to η^1 coordination, the 1a′ level gradually transforms from ($xz + yz$) to z^2, while the reverse transformation is occurring in the 3a′ level. The overlap of C_a with z^2 is much better than with ($xz + yz$) as shown by the increase in the Mo–C_a overlap population (0.41 in the η^2 structure and 0.71 in the η^1 configuration).

So far, the discussion has neglected the role played by the LUMO, 3a′. As the acyl group moves from η^2 to η^1 coordination, the energy of the LUMO drops precipitously as the antibonding overlap of O_a with ($xz + yz$) is removed. In the η^1 structure, the HOMO–LUMO gap is only 0.423 eV. A compound with such a small HOMO–LUMO gap would undoubtedly be high spin.

A curious thing has happened here. By conventional electron counting, we have gone from a stable "18-electron" η^2-acyl complex to an unstable "16-electron" η^1-acyl. Yet, as Figure 8 shows, electrons have *not* been lost on going from the η^2 to the η^1 structure. Rather, an empty *orbital* has been added to the bonding/nonbonding region. The η^1-acyl structure does require two more electrons to complete the "t_{2g}" shell. Therefore, the η^1 structure should be the preferred one for d^6, six-coordinate complexes.

Thus, these d^4, six-coordinate η^2-acyls are best thought of as stabilized 16e complexes similar to those with π-donor ligands recently discussed by Templeton et al.[57]

(57) Templeton, J. L.; Winston, P. B.; Ward, B. C. *J. Am. Chem. Soc.* **1981**, *103*, 7713.

On the Instability of $CpMo(CO)_2(\eta^2\text{-COR})$. As was pointed out in an earlier discussion, there are no known η^2-acyl complexes of the type, $CpMo(CO)L(\eta^2\text{-COR})$. Yet there is a growing set of isoelectronic, $L_5Mo(\eta^2\text{-COR})$ complexes (cf. Table V), where L_5 = $Tp(CO)_2$, $(PR_3)_3Cl(CO)$, $(PR_3)(Cl)_2(CO)_2$, etc. Are there one or more salient bonding features of the $CpMo(CO)_2^+$ fragment vis-ã-vis a $TpMo(CO)_2^+$ fragment, for example, which can account for the different positions of the equilibria shown in eq 10 and 11?

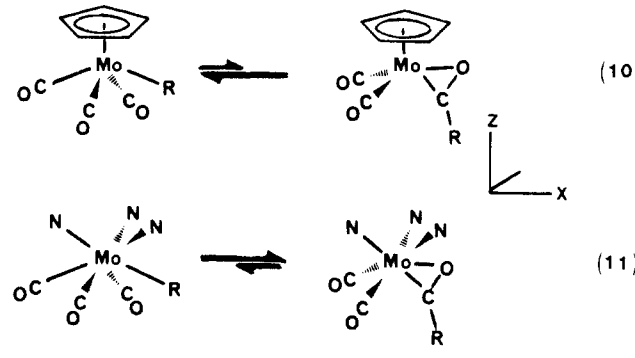

(10)

(11)

We have attempted to answer this question by using the EHMO model with R = H (eq 10 and 11) and the N-donors of the Tp ligand modeled with NCH groups. The fragments chosen for analyses were $L_3(CO)_2Mo$ (L_3 = $(HCN)_3$ or Cp) and (CO)(H) (for σ-H structures) or the HCO acyl group. The (CO)(H) FMO's are shown in Figure 5A. In this case, the FMO labeled "n–H" is the σ-donor orbital on CO perturbed by the H–1s orbital, and the "H + $\pi_\parallel$*" FMO is primarily localized as the H–1s orbital. With these fragments, the MO energy diagram of the σ-H structures resembles closely those of the η^2-acyl complexes.

The changes in the total energies calculated for the various structures are shown in Chart I. For the molecules with N-donor ligands, the σ-hydride tricarbonyl (hereafter referred to as the "σ-H" structure) is about 3 kcal/mol less stable than the η^2-acyl in its most stable configuration (ω = 45°) but is calculated to be more stable than the η^2-acyl in its least stable configuration (rotated 180°). For the Cp complex, the σ-H is calculated to be the most stable isomer by about 3 kcal/mol.

In view of the fact that $TpMo(CO)_3H$ has not been observed to rearrange to an η^2-formyl (see above), it is likely that the absolute numbers computed for the relative stabilities of the σ-H and η^2-acyl structures are incorrect. However, the calculations are in agreement with the empirical observation that $L_3(CO)_2$-

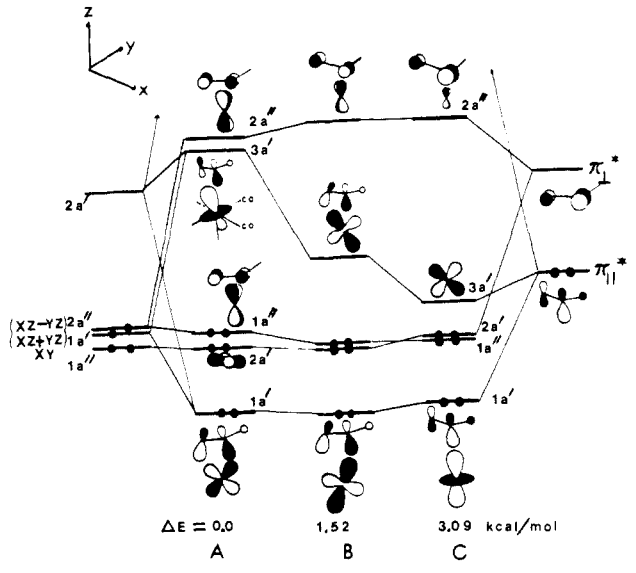

Figure 8. MO energy diagram showing the effects of transforming the HCO from $\eta^2 \rightarrow \eta^1$ in $(HCN)_3(CO)_2Mo(HCO)$: (A) η^2-HCO; (B) intermediate between η^2 and η^1; (C) η^1-HCO.

MoHCO complexes favor the η^2-acyl structure when L is a good σ-donor (e.g., Tp and PR_3), whereas the σ-H structure is favored when L_3 = Cp.

What factor or factors determine the relative stability orders? The Mulliken overlap populations (MOP) of the bonds of interest in these $L_3(CO)_2MoHCO$ compounds are listed in Table VI. First, we note that the σ-H $\rightarrow$ (η^2-acyl) transformation results in large decreases of the Mo–C and Mo–H MOP's. These decreases are largely compensated by the large increase in the C–H MOP as the C–H bond is formed. The sums of the MOP's of these bonds show a net decrease of 0.16 in the σ-H $\rightarrow$ (η^2-acyl) conversion for L = HCN, and a larger corresponding decrease (0.23) for L_3 = Cp. Thus, the Cp series suffers a greater net loss of bonding e density in these bonds than the N-donor series. The difference (0.23 − 0.16 = 0.07) is almost entirely due to the lower Mo–C MOP in the Cp η^2-acyl relative to the N-donor η^2-acyl (0.52–0.43 = 0.09; see Table VI).

The different relative stabilities of the σ-H and η^2-acyl structures in the Cp and N-donor complexes can thus be traced to the poorer Mo–C bonding in $CpMo(CO)_2(\eta^2\text{-HCO})$ vs. $(HCN)_3(CO)_2Mo(\eta^2\text{-HCO})$. This in turn is linked to the smaller *group* overlap integral between the π * FMO of the HCO fragment and the σ-hybrid FMO, 2a′ (Figure 8), in the Cp complex: $\langle \pi_\parallel^* | 2a' \rangle$ = 0.17 (Cp) vs. 0.25 (N_3).

The smaller overlap with the Cp fragment 2a′ FMO is a consequence of the different hybridizations in this orbital in Cp and N-donor fragments. The atomic orbital makeup of the 2a′ FMO in the Cp and N-donor fragments is shown in Scheme III. In both the Cp and N-donor fragments, a hybrid d_σ orbital points to the vacant coordination site. The major difference between the two fragments is the role played by an sp hybrid. In the N-donor fragment, the sp hybrid reinforces the outward pointing of the d_σ toward the vacant site. In the Cp complex, the sp hybrid turns the d_σ up toward the Cp ligand and away from the vacant site. Consequently, the overlap of the d_σ orbital with the η^2-acyl carbon is decreased in the Cp complex.

The cause of this behavior is quite straightforward. The sp combination hybridizes the d_σ orbital so as to minimize its antibonding interaction with the *σ-donors*. The σ-bonding properties of the N-donors are much more closely matched with the carbonyls than is the diffuse π-cloud of the Cp ring. In other words, the σ-bonding in the $N_3(CO)_2Mo$ fragment is more symmetric than in the $Cp(CO)_2Mo$ fragment.

All this is another way of saying that the donor electrons localized on the N_3 ligands promote octahedral coordination, whereas the diffuse π-cloud of the Cp ligand is less effective in this respect and is much happier with the seven-coordinate, four-legged piano stool structure. Other ramifications of this effect have been discussed elsewhere.[26,28,29]

Scheme III

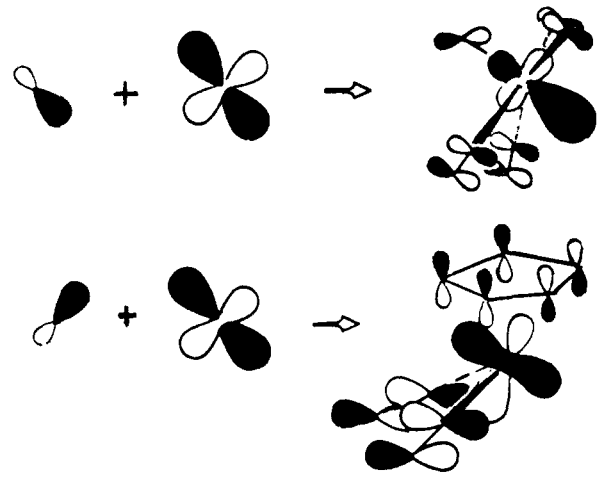

Conclusions

The $Tp(CO)LMo(\eta^2\text{-acyl})$ compounds prepared here are members of a growing class of six-coordinate, d^4 complexes. The structures of these compounds reveal interesting variations in the rotational orientation of the η^2-acyl group with respect to the L_5M fragment. The electronic factors governing these orientations have been explored theoretically in the framework of the EHMO model. A comprehensive view of the bonding of the η^2-acyl group in such compounds has been developed, and the insights of the factors governing their stability with respect to the seven-coordinate M(R)(CO) isomers should aid in further progress in this area.

Acknowledgment. We thank the National Science Foundation for support of this work (Grant CHE-8305235). K.-B.S. thanks the Department of Chemistry, the Graduate School, and the donors for James E. Harris and Rackham Fellowships. We are also grateful to Prof. F. Lalor for his correspondence and for sharing results prior to publication.

Appendix

EHMO calculations were performed with R. Hoffmann's programs ICON8 and FMO employing the weighted H_{ij} option.[58] The atomic parameters (H_{ii} and ζ) have been tabulated previously.[56] Unless specified otherwise, ligands in the L_5M fragment were placed on the $\pm x$, $\pm y$, and $-z$ axes at their appropriate distances: Mo–H, 1.70; Mo–CO, 2.0; Mo–C(acyl), 2.02; Mo–N, 2.10; Mo–P, 2.53; Mo–Cl, 2.50; C–O, 1.15; C–O(acyl), 1.22; C–H, 1.0; C–N, 1.16; P–H, 1.44; C–C(Cp), 1.43; Mo–Cp(centroid), 2.0 Å. The vector from Mo to the carbon of the η^2-acyl, C_a, subtended an angle of 21° with the $+z$ axis, and the M–C–O and M–C–H angles were 82.0° and 152°, respectively. In the "distorted" structures, the appropriate ligands were dropped 10° below the $\pm x$ or $\pm y$ axes. In the "piano stool" structures, the Mo–N and Mo–CO vectors subtended angles of 130° and 54°, respectively, with the $-z$ axis. The angles between the planes defined by the z axis and the Mo–L (L = CO and H) vectors were 90° (four-legged piano stools) or 120° (three-legged piano stools).

Note Added in Proof. It has come to our attention that $CpMo(CO)_2(CNR)^-$ reacts with MeI to give an η^2-iminoacyl (cf. eq 2) which reacts with phosphines to form the η^1-iminoacyl adduct (cf. eq 9a). See ref 59.

Supplementary Material Available: Complete tables of temperature factors, bond lengths and angles, and F_o vs. F_c for compounds **1–4** (50 pages). Ordering information is given on any current masthead page.

(58) Ammeter, J. H.; Burgi, H.-B.; Thibault, J. C.; Hoffmann, R. *J. Am. Chem. Soc.* **1978**, *100*, 3686.
(59) Adams, R. D.; Chodosh, D. F. *J. Am. Chem. Soc.* **1977**, *99*, 6544; *Inorg. Chem.* **1978**, *17*, 41.